Calibrating 1D hydrodynamic river models in the absence of cross-sectional geometry~~: A new parameterization scheme~~ using satellite observations of water surface elevation and river width

Liguang Jiang[1, 2], Silja Westphal Christensen[2, 3], Peter Bauer-Gottwein[2]

[1]School of Environmental Science and Engineering, Southern University of Science and Technology, Shenzhen, 518055, China

[2]Department of Environmental Engineering, Technical University of Denmark, 2800 Kgs. Lyngby, Denmark

[3]Department of Applied Mathematics and Computer Science, Technical University of Denmark, 2800 Kgs. Lyngby, Denmark

Correspondence to: Liguang Jiang (jianglg@sustech.edu.cn)

Abstract. Hydrodynamic modeling has been increasingly used to simulate water surface elevation which is important for flood prediction and risk assessment. Scarcity/inaccessibility of in-situ bathymetric information has hindered hydrodynamic model development at continental-global scales. Therefore, river cross-section geometry has commonly been approximated using highly simplified generic shapes. Simultaneous calibration of shape parameters and roughness is difficult, because often there are trade-offs between them. Instead of parameterizing cross-section geometry and hydraulic roughness separately, ~~However, strong correlations appear between cross-section shape parameters and hydraulic roughness in a hydraulic inversion approach. T~~this study introduces a ~~novel~~ parameterization of 1D hydrodynamic models ~~that reduces ambiguity~~ by combining cross-section geometry and roughness into ~~a~~ one conveyance parameter. Flow area and conveyance are expressed as power-law functions of flow depth, and ~~thus~~ they are ~~assumed~~ found to be linearly related in log-log space at reach scale. Data from a wide range of river systems show that the linearity approximation is globally applicable. Because the two are expressed as power-law functions of flow depth, no further assumptions about channel geometry are needed. Therefore, the hydraulic inversion approach allows for calibrating flow area and conveyance curves in the absence of direct observations of bathymetry and hydraulic roughness. Its feasibility and performance are illustrated using satellite observations of river width and water surface elevation in the Songhua River, China. Results show that this approach is able to reproduce water level dynamics with root mean square error value of 0.44 m and 0.50 m at two gauging stations, which is comparable to that achieved using a standard calibration approach. In summary, this study puts forward an alternative method to parameterize and calibrate river models using satellite observations of river width and water surface elevation.

1 Introduction

30 Hydrodynamic modeling of rivers is important for quantitative assessment of river flow and water level dynamics and, critically, for risk assessment and flood prediction. It has been widely used for many applications, such as estimates of hydraulic parameters (e.g. water surface elevation (WSE), longitudinal profile, velocity), flood forecasting, inundation estimation, risk assessment, river maintenance, etc. (Andreadis and Schumann, 2014; Bates et al., 2014; Bierkens, 2015; Blöschl et al., 2015; Jiang et al., 2020). Nowadays, in the era of big data, earth observation datasets, cloud computing, and

35 complex modeling platforms are available for better simulations of WSE at different scales (Fleischmann et al., 2019; Gleason and Durand, 2020; Ward et al., 2015).

Traditional hydrodynamic modeling approaches require detailed river channel bathymetry, which is usually represented by cross-sectional geometry. There are, however, only a limited number of rivers, for which the surveyed cross-sectional geometry is available. The challenge that arises in many studies is how to approximate the channel geometry. This is a

40 common problem facing the scientific community. A common approach is to parameterize channel geometry as a simple shape, e.g. a rectangle or triangle (Garambois et al., 2017; Jiang et al., 2019; Neal et al., 2012; Schneider et al., 2017). Instead of rectangular or triangular shapes, Dingman (2007) and Neal et al. (2015) used a power function (bankfull width and depth are required) to represent channel shape variability between the limiting cases of rectangular and triangular shape. However, Neal et al. (2015) used a uniform shape instead of varying shapes along the channel. Similar parameterizations of

45 cross section shapes were used in Mejia & Reed (2011), and the effect of assumed shapes on simulated flows was investigated. Some studies estimated river bathymetry using global DEMs combined with an assumed simplified shape (e.g. rectangle) of the submerged portion of the river. Domeneghetti (2016) used DEM data to infer the river bathymetry based on width-elevation relationships of high flow and low flow, respectively. Similarly, a few studies infer bathymetry from water surface height and width by fitting the relationship between the two. Obviously, the success of this approach depends on the

50 channel exposure (Mersel et al., 2013). Moreover, combinations of remote sensing data and empirical statistical relationships or data assimilation approaches have also been used to infer effective bathymetry (Brisset et al., 2018; Dey et al., 2019; Durand et al., 2008; Fonstad and Marcus, 2005; Grimaldi et al., 2018; Larnier et al., 2020; Legleiter, 2015; Moramarco et al., 2019; Schaperow et al., 2019). For instance, Durand et al. (2008) estimated bathymetric depth and slope by assimilating synthetic WSE data from the Surface Water and Ocean Topography (SWOT) mission into the LISFLOOD-FP hydrodynamic

55 model. Larnier et al. (2020) also applied data assimilation to infer effective bathymetry from synthetic SWOT altimetry measurements within an inverse framework. Here we do not comprehensively review bathymetry estimation using upcoming SWOT mission data. Instead, we refer the reader to Biancamaria et al. (2016) and Gleason & Durand (2020) for a broader overview.

In addition to the channel bathymetry, channel roughness is another factor that is important to simulate flow dynamics

60 with sufficient accuracy (Bates et al., 2014; Neal et al., 2015). Usually, a uniform value is adopted to represent channel/floodplain roughness although large heterogeneity of river morphology exists in most cases (Annis et al., 2020;

Jiang et al., 2020; Pappenberger et al., 2007; Schumann et al., 2007). When calibrating channel geometry parameters along with roughness parameters, strong parameter correlation appears between cross section shape (wetted perimeter) and hydraulic roughness (Jiang et al., 2019). That is, the roughness parameter will be "effective", not only representing the friction but also compensating for inaccurate geometry, which affects the hydraulic resistance through the wetted perimeter. Therefore, roughness and geometry parameters trade-off against each other, which has been widely reported (see Garambois & Monnier (2015) and references therein).

In order to address this ambiguity reduce parameter correlation in hydraulic inverse problems, we put forward a method to parameterize and calibrate the 1-D river models in a different way. Instead of roughness and geometry, flow area and conveyance curves as functions of flow depth are estimated in an inverse modeling workflow. In this way, only the dependence of area and conveyance on flow depth is estimated, regardless of the detailed channel shape and roughness. This paper illustrates this approach for the calibration of an 1D MIKE Hydro River model (DHI, 2017) to simulate WSE dynamics, using satellite observations of WSE and river width as observations. The novelty is to use power-law relationships between flow area / conveyance and flow depth in a hydraulic inversion without detailed cross-sectional data or assumption of any specific cross-sectional shape. Therefore, this approach is fundamentally different from previous studies, and provides an alternative way for hydrodynamic model calibration.

2 Methods

2.1 Theoretical background

Flow in open channels can be described by the continuity equation and momentum equation, known as the de Saint-Venant equations (Chow, 1959):

$$\frac{\partial A(d)}{\partial t} + \frac{\partial Q}{\partial x} = 0 \tag{1}$$

$$\frac{\partial Q}{\partial t} + \frac{\partial}{\partial x}\left(\frac{Q^2}{A(d)}\right) + gA(d)\frac{\partial d}{\partial x} - gA(d)\left(S_0 - S_f\right) = 0 \tag{2}$$

where: A is the cross-sectional area; Q is the discharge; d is the flow depth; S_0 is the slope of the channel bottom; S_f is the friction slope; g is the gravity acceleration; t is time and x is chainage, i.e. the distance along the channel.

Equations (1) and (2) compose the 1-D dynamic wave model. In the absence of cross-sectional geometry, there are five unknowns in this model, i.e. A, two variables (Q, and d) and three parameters (A, S_o, and S_f). To effect a solution of Q and d, information about channel geometry and friction slope is required. Flow area A and channel slope S_o can be obtained once bathymetry is known. Friction slope S_f can be approximated using the Manning formula or the Chézy formula (Chow, 1959).

Here, we express friction slope as a function of conveyance (K) and discharge (Q) using Manning's equation

$$Q = K S_f^{\frac{1}{2}} \tag{3}$$

$$K = \frac{1}{n} A \, R^{\frac{2}{3}} \tag{4}$$

where, n is the Manning roughness coefficient and R is the hydraulic radius. The conveyance is a measure of water carrying capacity of a cross section ~~since it is directly proportional to discharge~~ (Chow, 1959).

Substituting for S_f, the momentum equation is written as:

$$\underbrace{\frac{\partial Q}{\partial t} + \frac{\partial}{\partial x}\left(\frac{Q^2}{A(d)}\right)}_{inertia\ terms} + \underbrace{\underbrace{gA(d)\frac{\partial d}{\partial x} - \overbrace{gA(d)\left(S_0 - \frac{Q^2}{K^2(d)}\right)}^{Kinematic\ wave}}_{Diffusive\ wave}}_{Dynamic\ wave} = 0 \tag{5}$$

This version of the momentum ~~equation~~ Eq. (5) indicates that, in steady state (for both kinematic wave and diffusive wave), $K(d)$ is much more sensitive than $A(d)$, and $A(d)$ appears only when the flow accelerates or decelerates.

2.2 Parameterization of flow area and conveyance curves

 Equations (1) and (5) provide two equations with still five unknowns, i.e. two variables ($A$$Q$ and d, Q), and three parameters$d$, (A, S_o, and K). However, K and A are related to flow depth, d. If K and A can be expressed as functions of d, Q and d can be solved for, given the slope S_o but without the need for detailed information on cross-sectional shape and roughness. The hydraulic geometry relations are widely used to relate the water surface width, average depth, and average velocity to discharge since it was introduced by Leopold and Maddock in 1953 (Bjerklie et al., 2005; Dingman, 2007; 105 Ferguson, 1986; Gleason, 2015; Leopold and Maddock, 1953). Dingman (2007) has derived explicit equations for the exponent and coefficients in the power-law function, explaining the variation of hydraulic geometry in different rivers. In some way analogous to the at-a-station power-law of hydraulic geometry, power function relationships that relate flow area A and conveyance K to flow depth d of a cross section can be written, respectively, as (Chow, 1959; Garbrecht, 1990):

$$A(d) = a \, d^\beta \tag{6}$$

$$K(d) = c \, d^\delta \tag{7}$$

$$d = H - Z_0 \tag{8}$$

where, a, β, c and δ are empirical coefficients; H and Z are WSE and channel datum, i.e. water surface elevation for zero flow.

Transforming ~~equations~~ Eq. (6) and Eq. (7) into log-log space, we can write the following linear relationships:

$$\log A(x,t) = \alpha(x) + \beta(x) \log d(x,t) \qquad (9)$$

$$\log K(x,t) = \gamma(x) + \delta(x) \log d(x,t) \qquad (10)$$

where $\alpha = \log(a)$ and $\gamma = \log(c)$. This relationship is investigated for different rivers having a wide range of river width (three orders of magnitude) to show its validity for real-world rivers. Note that, these six rivers are used simply due to the availability of cross-section data (see a map of rivers and cross sections in Figure A1Fig. S1). Strong positive linear

relationships are readily revealed by plotting the logarithmic $A \sim d$, and $K \sim d$ pairs for any given cross section below bankfull depth (Figure 1Figure 1). A discontinuity may occur if significant flood plain exists as the case of the Yellow River (Figure 1Figure 1d). Chow (1959) and Garbrecht (1990) suggested using separate functions to approximate the hydraulic properties below and above bankfull depth. In this initial study, one single power-law function is used. Note that the conveyance changes with the Manning's number, but the linear relationship holds (Fig. S2Figure A2). To calculate

conveyance, spatially varying, randomly distributed Manning's number ranging between 0.015 and 0.05 are used to mimic real-world rivers instead of unrealistic uniform values along the whole reach. A uniform Manning's number results in a much stronger linear relationship (Figure A2 andFigure A3Figures S2 and S3).

Figure 1. Plots of flow area and conveyance against flow depth in log-log space. In each plot, dots in the same color are from one certain cross section. Linear relationships between logarithmic area / conveyance and depth are estimated for each cross section, i.e. in an "at-a-station" manner. The median value of slopes of linear regression is given in each plot. In total, there are 60, 70, 335, 98, 51, 165 cross sections spaced at 2.5 km, 6 km, 1 km, 8 km, 150 m and 300 m, respectively, for (a) Changjiang, (b)Songhua, (c) Po, (d) Yellow, (e) Åmose, and (f) Vejle rivers. Please refer to **Figure A1**~~Figure S1~~ for a detailed map. Note that, Manning's number used for calculation of conveyance for each cross section is randomly generated between 0.015 and 0.05.

However, there are four more parameters (i.e. α, β, γ, δ) for each cross section to be estimated. Due to the linear nature of logarithmic pairs of (A, d) and (K, d), a linear relationship can be derived between the ~~logarithmic~~ $A \sim d$ and $K \sim d$ curves for each individual cross section. The mathematical derivations are given in Appendix A (Eqs. (A1) – (A4)). Unfortunately,

140 the linear relationships are varying with cross sections, meaning many coefficients (intercept and slope of the linear function as shown in Eqs. (A2) and (A4)) to be determined. ~~as shown in the data (Figure 2).~~ By fitting a linear function to the cross-sectional parameter pairs ($\alpha \sim \delta$ and $\beta \sim \gamma$) derived from observed data at the reach scale as shown in Figure 2~~Therefore,~~, the flow area and conveyance curves for all cross sections can be connected by:

$$\alpha = p_1 + p_2 \gamma \qquad (11)$$

145

$$\beta = p_3 + p_4 \delta \qquad (12)$$

It should be noted that the linear relationships (i.e. ~~equations~~ Eq. (11) and Eq. (12)) are only valid at river reach scale instead of individual cross sections. In this way, we can simplify the hydraulic inverse problem by tying there parameters together, i.e. halving the number of fitting parameters. ~~~Interestingly,~~ p_1, p_2, p_3, and p_4 are nearly constant independent of rivers although marginal deviations exist (Fig. ~~S4~~Figure A4). As shown in Figure 2~~Figure 2~~, when pooling cross sections of

150 all rivers together, a clear linear trend shows up for both $\alpha \sim \gamma$ and $\beta \sim \delta$. This indicates that parameters p_2 and p_4 should vary in a very narrow range around 1.0 for all rivers; And parameters p_1 and p_3 should be allowed to be slightly varying around -1.4 and -0.7 to adapt to individual rivers. Thus, there are two spatially varying parameters (i.e. γ, δ~~α, β~~) and four uniform parameters (i.e. $p_1 \sim p_4$) in addition to bed slope S_o (calculated from datum Z_0) to be constrained in order to solve Q and d. Therefore, a new parameterization of a river model can be written as:

155

$$\log_{10}\big(K(x,t)\big) = \gamma(x) + \delta(x) \log_{10}\big(d(x,t)\big) \qquad (13)$$

$$\log_{10}\big(A(x,t)\big) = \big(p_1 + p_2\,\gamma(x)\big) + \big(p_3 + p_4\,\delta(x)\big) \log_{10}\big(d(x,t)\big) \qquad (14)$$

with p_1, p_2, p_3, and p_4, close to - 1.4, - 0.7, 1.0 and 1.0, respectively.

Figure 2. Linear relationship between α~~alpha~~/β ~~beta~~ and γ~~gamma~~/δ ~~delta~~. Each dot represents one cross section of a certain
160 river. Dots of the same color are from the same river. Manning's number for each cross section is randomly generated

between 0.015 and 0.05. Note that, the best-fit line for each river is slightly different. The relationship using a uniform Manning's number of 0.03 is also given in ~~Figure S3~~**Figure A3**. Individual fitting lines are shown in **Figure A4**~~Figure S4~~.

~~2.3 Parameter calibration~~

~~Hydraulic parameter calibration is essentially an inverse problem that is often solved using the least squares approach. In this study, a non-linear least squares solver, i.e. the Levenberg-Marquardt algorithm, is used to solve the calibration problem by minimizing the objective function. An ensemble of 10 calibrations with different starting models are conducted to avoid local minima.~~

~~Considering the large number of parameters (p_1, p_2, p_3, and p_4, and spatially varying Z_0, γ and δ), regularization is used to stabilize the ill-posed problem (Pereverzyev et al., 2006; Schmidt, 2005). In this work, the Tikhonov type regularization is applied and the objective function is formulated following (Aster et al., 2018):~~

$$\min_{\mathbf{x}} \phi(x) = \min_{\mathbf{x}}(\|r(\mathbf{X})\|_2^2 + \lambda^2\|L\mathbf{X}\|_2^2) \tag{15}$$

~~where **X** is vector containing the parameters described above; r(**X**) is the residuals between model predictions and observations (i.e. water level and width); λ^2 is the regularization parameter that controls the strength of the regularization; and L is a roughening matrix that constrains the model space. In this study, the first-order regularization is used to smooth the model space. It is a finite difference approximation to the first derivative of the model. The larger λ is, the smoother the model parameters are. For detailed objective function and model calibration, please refer to the supporting information (Text S2).~~

~~Essentially, by optimizing Eq. (15) using satellite-derived observations of WSE and river width, we calibrate the two curves, i.e., the relationships between flow area / conveyance and depth as described by equations (13) and (14).~~

3 Case study

To test whether this approach is able to reproduce realistic flow area and conveyance curves as well as WSE using remote sensing data, we use the Songhua River as a test site ~~(Figure S5)~~. Below are the descriptions of test site, data sets, model setup and calibration procedures.

3.1 Study site

Songhua River ~~It~~ is the longest tributary of the Amur (or Heilong Jiang), and ~~somewhat~~ representative of large rivers worldwide. It allows testing the approach using satellite data sets, such as altimetry and imagery, which will be available simultaneously from the future SWOT mission (Biancamaria et al., 2016).

The river has two sources, i.e. Nenjiang and Second Songhua rivers, originating from the Greater Khingan Range in the north and the Paektu Moutain in the south, respectively, and drains an area of 556 800 km². At Sanchahe, two rivers merge

into one, called Songhua River. It runs 840 km northeastward before emptying into the Amur River (Songliao River Conservancy Commission, 2004, 2015). In this study, we focus on the middle reach of the main Songhua River, between Harbin and Jiamusi (Figure 3). The reason we selected this reach is twofold: firstly, it is wide enough (700 m on average) to have high-quality altimetry data as shown in previous study (Jiang et al., 2017) and secondly, we have access to in-situ data of several hydrometric stations across this region. This reach covers an area of 138 500 km^2 and stretches 433 km long. The elevation difference of this reach is about 45 m, resulting an average slope of 0.1 m km^{-1}. The first 222 km drains through hilly terrain with a gentle slope of 0.05 m km^{-1} while the downstream reach is narrower and deeper. The mean discharge at downstream is about 1175 m^3 s^{-1}. The river is frozen in winter and reaches its maximum flow in summer.

Figure 3. Overview of the study area. The studied reach is 433 km long between Harbin and Jiamusi. There are five major tributaries recharging the main river. There are 23 cross sections evenly distributed along this reach as shown in the lower map.

3.2 Data sets and model setup

A 1D river model is built using the MIKE Hydro River software (DHI, 2017). The river network is set using the center line of the reach, while cross sections are equally distributed along the 433 km reach as in Jiang et al. (2019). Daily discharge at Harbin hydrometric station is used as the upstream boundary while a uniform flow depth rating curve is set as downstream boundary. Inflows of three tributaries are from gauging records while remaining tributary inflows are simulations from a hydrological model (Jiang et al., 2019). The only available in-situ surveyed cross sections are from the late 1990s. These "real" area curves are only used to validate the calibration results.

WSE and river width derived from CryoSat-2 altimetry and Landsat imagery are used as observations in the calibration. CryoSat-2 altimetry is distinctive due to several new features, most importantly the orbit configuration. Specifically, CryoSat-2 with its drifting ground track pattern results in an entirely different sampling pattern. The small inter-track spacing of 7.5 km enables dense sampling of rivers and thus provides longitudinal water level profiles. Although these profiles are not snapshots of river level at a given time, they are still useful for resolving local hydraulic characteristics (Jiang et al., 2019; Schneider et al., 2018). CryoSat-2 observations are the same as those used in Jiang et al. (2019), covering the period of 2010-2014. Widths are derived using the RivWidthCloud algorithm in Google Earth Engine (Yang et al., 2020). We used Landsat 5 and Landsat 8 images and selected images to avoid cloud cover and obtain an even distribution in time. Specifically, if the river is cloud-free in a given image, it is selected regardless of the cloudiness of other parts. Images collected from December to early April are excluded. In total, 37 Landsat 5 images and 15 Landsat 8 images are used and provided 10022 individual width observations. The temporal and spatial distribution of WSE and widths observations is shown in Figure B1.

For the purpose of validation, gauging records of water level and discharge at Tonghe and Yilan (Figure 3. Overview of the study area. The studied reach is 433 km long between Harbin and Jiamusi. There are five major tributaries recharging the main river. There are 23 cross sections evenly distributed along this reach as shown in the lower map.Figure 3) are collected. Moreover, WSE datasets derived from Jason-2 at two virtual stations (Figure 3) are also included for extensive validation. Because the river is completely frozen, altimetry does not provide realistic WSE observations during the winter. Therefore, we only consider the ice-free period (April to October) in this study. To compare results with the previously published calibration approach (e.g. simultaneous calibration of roughness and cross-sectional shape parameters), we also extract model simulations from our previous work (Jiang et al., 2019). Specifically, water level simulations from model calibration S1 (refer to (Jiang et al., 2019)) are used for a fair comparison given that both calibrations use the same amount of CryoSat-2 WSE data.

~~We use the same reach (433 km evenly divided by 23 cross sections) and boundary conditions as used in Jiang et al. (2019). Specifically, observed discharge is used as the upstream boundary while normal depth is set as downstream boundary. Inflows of three tributaries are from gauging records while remaining tributary inflows are simulations~~

~~from a hydrological model (Jiang et al., 2019). The only available in-situ surveyed cross sections are from the late 1990s. These "real" area curves are only used as a benchmark for the calibration results. The validation is focused on the reproduction of WSE at two independent gauging stations as well as altimetry virtual stations. Currently, satellite altimetry derived WSE and satellite imagery derived river width are widely used data sets to study river dynamics (Alsdorf et al., 2007). Therefore, the calibration data sets used are WSE and water surface width, which are derived from CryoSat-2 altimetry and Landsat imagery, respectively. CryoSat-2 observations are the same as those used in Jiang et al. (2019) while widths are processed using the RivWidthCloud algorithm in Google Earth Engine (Yang et al., 2020). The experiments are conducted under several scenarios to test the capability of different data sets, i.e. WSE only, width only, and both WSE and width combined (see Text S3 for further explanation). Spatio-temporal distribution of both data sets is shown in Fig. S6. We use the MIKE Hydro River model to implement this approach (see Text S2 for more details).~~ **3.3 Parameter calibration**

Hydraulic parameter calibration is essentially an inverse problem that is often solved using the least squares approach. Considering the large number of parameters (p_1, p_2, p_3, and p_4, and spatially varying Z_0, γ and δ), regularization is used to stabilize the ill-posed problem (Pereverzyev et al., 2006; Schmidt, 2005). In this work, the Tikhonov type regularization is applied and the objective function is formulated following (Aster et al., 2018):

$$\emptyset(\mathbf{X}) = \lambda \, misfit + (1 - \lambda) \, reg \tag{15}$$

$$misfit = w \left(\frac{1}{N_h} \left(\frac{h_s - h_o}{\sigma_h} \right)^2 \right) + (1 - w) \left(\frac{1}{N_b} \left(\frac{b_s - b_o}{\sigma_b} \right)^2 \right) \tag{16}$$

$$reg = \lambda_\gamma \left(\frac{1}{N} \left(\frac{L\,\gamma}{\sigma_\gamma} \right)^2 \right) + \lambda_\delta \left(\frac{1}{N} \left(\frac{L\,\delta}{\sigma_\delta} \right)^2 \right) + \lambda_{p1} \left(\frac{p_1 + 1.4}{\sigma_{p1}} \right)^2 + \lambda_{p2} \left(\frac{p_2 - 1}{\sigma_{p2}} \right)^2 + \lambda_{p3} \left(\frac{p_3 + 0.7}{\sigma_{p3}} \right)^2$$

$$+ \lambda_{p4} \left(\frac{p_4 - 1}{\sigma_{p4}} \right)^2 + (1 - \lambda_\gamma - \lambda_\delta - \lambda_{p1} - \lambda_{p2} - \lambda_{p3} - \lambda_{p4}) \left(\frac{1}{N} \left(\frac{L\,z}{\sigma_z} \right)^2 \right) \tag{17}$$

where $\mathbf{X}$ is vector containing the parameters γ, $\boldsymbol{\delta}$, p_1, p_2, p_3, p_4, and z; λ is a weighting factor balancing the regularization and data fitting error; w is a weighting factor balancing the fitness of water level and width; h_s, h_o, N_h, σ_h are simulated water level, observed water level, number of water levels, and the uncertainty of observed water level; b_s, b_o, N_b, σ_b are simulated width (calculated as the derivative of flow area with respect to depth in the model), observed width, number of widths, and the uncertainty of observed width; λ_γ, λ_δ, λ_{p1}, λ_{p2}, λ_{p3}, λ_{p4} are regularization parameters; σ_γ, σ_δ, σ_{p1}, σ_{p2}, σ_{p3}, σ_{p4} and σ_z are the a priori standard deviations indicating how uncertain the parameters are a priori; N is the number of cross sections; and L is the first-order regularization roughening matrix, which is a finite-difference approximation to the first derivative of the model:

$$L = \begin{bmatrix} 1 & -1 & & & \\ & 1 & -1 & & \\ & & \ddots & \ddots & \\ & & & 1 & -1 \\ & & & & 1 & -1 \end{bmatrix}$$

In this case study, the weighting factor λ is set as 0.8 based on a trial-and-error method. The weighting factor w is set to 0.5, i.e. water level and river width observations are equally important. The uncertainties of water level and width are 0.5 m and 99 m according to (Jiang et al., 2017) and (Yang et al., 2020), respectively. The a priori standard deviations of σ_y and σ_δ are 0.7 and 0.4, respectively, which are similar for relatively large rivers (see γ and δ distributions in Figure S2). The a priori standard deviations of p_1, p_2, p_3, p_4 are chosen as 0.02, 0.01, 0.02, and 0.01, respectively, given that those parameters vary slightly (see Figure A3 and Figure A4). The datum Z_0 is the sum of parameter z and a constant value which is estimated from the average water level subtracting the depth of 5 m. The a priori standard deviation of z is 0.5 m. The regularization parameters, i.e. λ_y, λ_δ, λ_{p1}, λ_{p2}, λ_{p3}, λ_{p4} are empirically set as 0.1, 0.1, 0.15, 0.15, 0.15, 0.15, respectively, to achieve appropriate smoothness.

We use the Levenberg-Marquardt (LM) algorithm (Marquardt, 1963) to optimize the objective given above. The LM algorithm is an iterative search process that proceeds towards a minimum of the objective function value. In each iterative step, the Jacobian of the objective function is calculated. However, computing the Jacobian in every iteration is computationally expensive and in some cases the Jacobian does not change and thus, evaluation of the Jacobian can be unnecessarily costly. Instead, Broyden's rank-one update of the Jacobian (Broyden, 1965) is more efficient (Madsen et al., 2004). We use the Immoptibox toolbox (Nielsen and Völcker, 2010) to optimize the objective function. Given that LM finds a local minimum and cannot guarantee the global minimum, an ensemble of 10 calibrations is carried out with different initial guesses to avoid convergence to a local minimum. For each calibration, the number of model runs is around 200. The time consumed for this optimization is a few hours (1 ~ 4 hours). The calibrations were conducted on a windows server 2016 (Inter® Xeon® Gold 6154 CPU @ 3 GHz, 2993 Mhz) using 4 cores.

The calibration is implemented in Matlab. C# scripts are used to modify and dump MIKE Hydro River parameters and simulation results. The power-law relationships are an integral part of the MIKE Hydro River model. Specifically, for each iteration of the optimization, the updated parameters by LM algorithm as well as the calculated flow area and conveyance relationships are passed to a C# script that updates the setup of the MIKE Hydro River model. Then the model is executed, and the results are passed on to Matlab. Essentially, by optimizing Eq. (15) using satellite derived observations of WSE and river width, we calibrate the two curves, i.e., the relationships between flow area / conveyance and depth as described by equations (13) and (14) for each cross section along the reach.

3.4 Calibration scenarios

To test the capability of different data sets to constrain model parameters, three basic scenarios are used based on the type of data sets. That is, calibration #1 uses altimetry derived WSE only; calibration #2 uses imagery derived width only; and calibration #3 uses both WSE and width. Given that width observations are of very high spatial resolution (30 m interval), three scenarios of width observations are also designed (Table 1). Specifically, width is sampled at course spatial resolution by randomly selecting one observation for each 2 or 5 km reach regardless of the timing. Given that only 261 observations of WSE are available, no further exploration of the effect of WSE data is performed. Therefore, in total, we test 7 scenarios of observations to calibrate the model (Table 1).

Table 1. Details of the calibration scenarios with different data sets.

Scenario	Description	Num. of WSE	Num. of width
Calibration #1	Calibration with WSE observations only	261	0
Calibration #2a	Calibration with one width per 5 km	0	88
Calibration #2b	Calibration with one width per 2 km	0	219
Calibration #2	Calibration with width observations only	0	10022
Calibration #3a	Calibration with WSE and one width per 5 km	261	88
Calibration #3b	Calibration with WSE and one width per 2 km	261	219
Calibration #3	Calibration with WSE and width observations	261	10022

4 Results

Results prove the~~that it is possible to calibrate~~ ~~feasibility of calibration of~~ spatially varying area-depth curves using solely satellite data sets. Figure 4~~Figure 4~~ depicts the calibrated area-depth curves at 23 cross sections under the three scenarios. Two metrics are used to evaluate the performance alongside the plots. RMSE describes the error of the calibrated $\log Area$ vs $\log depth$ relationship, and coverage is defined by the percentage of real data that fall within the confidence interval. Compared to the curves derived from surveyed cross sections, the calibrated ones are reasonably close at most locations. Most of the largest errors occur at cross sections 4-6, where the Dadingzishan reservoir (chainage 20 - 90 km) is located and not modelled. Interestingly, ~~either~~both WSE alone and ~~or~~ river width alone ~~is~~are able to constrain the model to a certain degree (Figure 4~~Figure 3~~)~~., and calibrated model can reproduce WSE with similar RMSE at two gauging stations (see Fig. S7).~~ However, calibration #1 (WSE only) has slightly larger spread especially for small depth. The average RMSE and coverage are 0.42 and 16%. ~~c~~Calibration #2 (width only) tends to overestimate flow area, which is significant for downstream cross sections. The corresponding average RMSE and coverage are 0.34 and 8%. ~~has larger spread;~~ ~~c~~Calibration #3 (both WSE and width) shows the best match (smaller RMSE and larger coverage) with the observed cross

sections (Figure 4Figure 3). Moreover, very dense observations of width (one per 30 m#2 and #3) do not improve the calibration results compared to less dense ones (one per 5 km, Fig. S8#2a and #2b, #3a and #3b) although high resolution imagery (30 m) can provide plenty of width observationscalibrations #2 and #3 result in narrower confidence intervals (Figure B2 and Figure B3). It should be noted that the reservoir in the upstream portion (chainage 20 - 90 km) is not modelled, which explains the large uncertainty of the curves in the upstream.
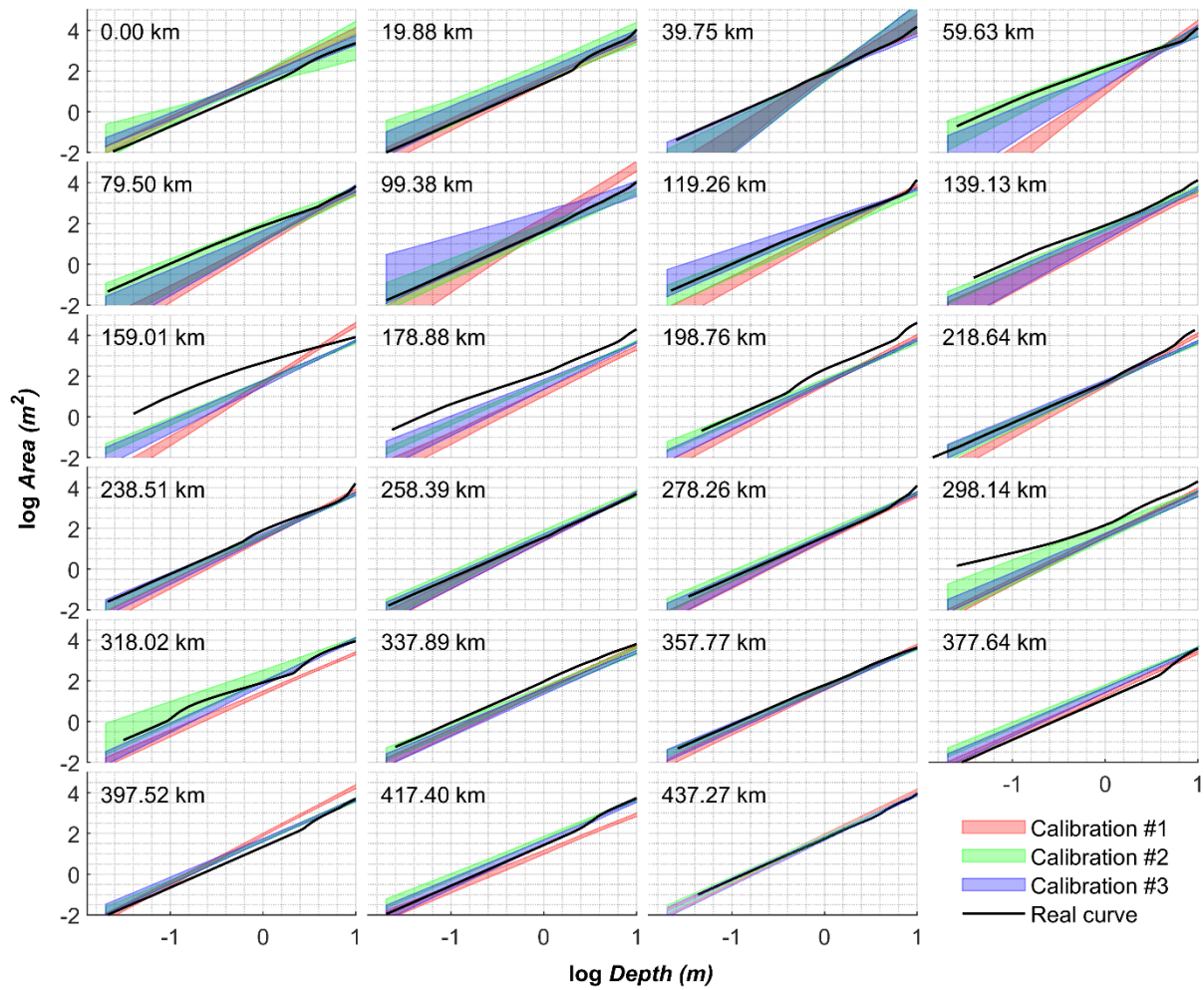
325
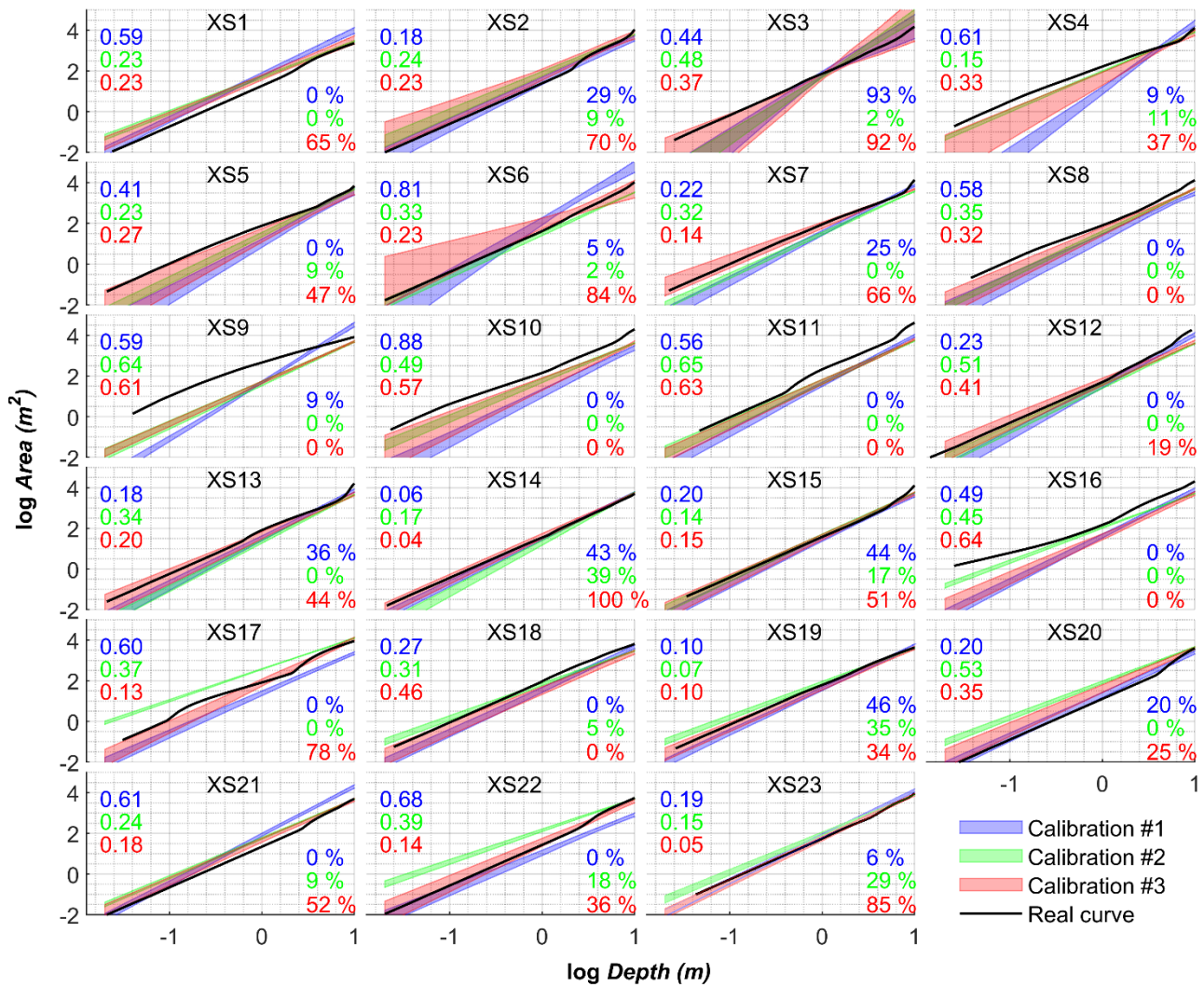
Figure 4~~3~~. Calibrated area-depth curves at 23 cross sections (~~chainage~~ number is given in each plot). Three scenarios are shown, i.e. calibration with water surface elevation data only (calibration #1), river width only (calibration #2), and both water surface elevation and width (calibration #3), respectively. Please refer to Table 1 for more information. The color band represents the mean ± standard deviation based on an ensemble of 10 calibrations. RMSE and coverage (percentage of real data falling into the calibrated interval) of calibrated curves against real data are reported on the left and right sides of each plot, respectively. Font color is consistent with the curve color.

Figure 5 Shows the performance of each calibration scenario in terms of accuracy of simulated water level. Similarly, models calibrated with either WSE (calibration #1) or width (calibration #2) can reproduce WSE with similar RMSE at two gauging stations. However, calibration #2 shows larger RMSEs and wider ranges than calibration #1, especially at the Yilan station. In contrast, calibration #3 is more stable, resulting in smaller RMSEs and narrower ranges. This is in line with the well calibrated area-depth curves at cross sections (XS12, XS13, XS17, XS18) nearby the two stations (refer to Figure 3 for the locations). Regarding the scenarios using width observations, calibrations #2a and #2b show a very wide range of RMSE,

indicating that models are not well-constrained. This is evidenced by the poorly calibrated area-depth curves (e.g. wider
340 color bands of XS17 and XS18) shown in Figure B2.
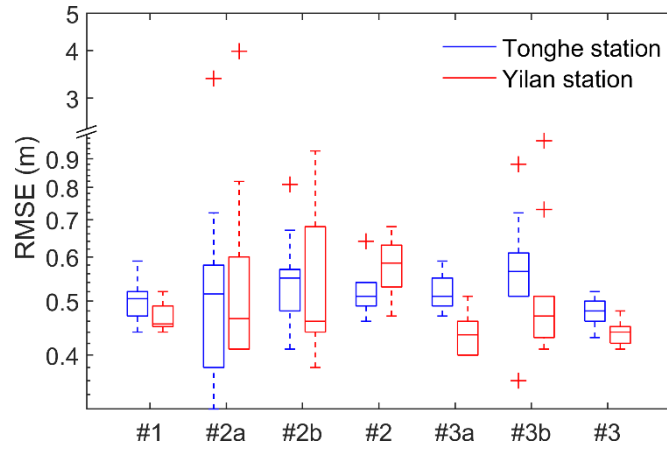
Figure 5. Boxplots of evaluations of simulated water level against in-situ gauging records at two gauging stations. Calibration scenarios indicated on the x-axis are referred to **Table 1**. Note that, the y-axis is in log scale.

~~Results prove the feasibility of calibration of spatially varying area-depth curves using solely satellite data sets. Figure 4~~
345 ~~depicts the calibrated area-depth curves at 23 cross sections under the three scenarios. Compared to the curves derived from~~
~~surveyed cross sections, calibrated ones are reasonably close at most locations. Interestingly, either WSE or river width is~~
~~able to constrain the model to a certain degree (Figure 3), and calibrated model can reproduce WSE with similar RMSE at~~
~~two gauging stations (see Fig. S7). However, calibration #2 (width only) has larger spread; calibration #3 (both WSE and~~
~~width) shows the best match with the observed cross sections (Figure 3). Moreover, very dense observations of width (one~~
350 ~~per 30 m) do not improve the calibration result compared to less dense one (one per 5 km, Fig. S8) although high-resolution~~
~~imagery (30 m) can provide plenty of width observations. It should be noted that the reservoir in the upstream portion~~
~~(chainage 20 – 90 km) is not modelled, which explains the large uncertainty of the curves in the upstream.~~ The calibrated
model can reproduce WSE reasonably well when compared with independent data sets. Figure 6 ~~Figure 4~~ shows simulated
WSE using calibrated curves shown in~~ ~~Figure 4~~Figure 3~~. Overall, the accuracy of simulation is acceptable. RMSE is about
355 50 cm and 44 cm at Tonghe and Yilan stations, respectively. The accuracy is ~~and~~ comparable to what was achieved using a
different approach, which simultaneously calibrates cross-sectional shape parameters and roughness (Jiang et al., 2019). A
careful comparison indicates that the simulations are slightly better than those reported in Jiang et al. (2019)~~, especially~~ for
low WSE (Figure 6). Compared to Yilan, Tonghe shows slightly higher RMSE (Figure 6~~Figure 4~~) due to the underestimation
of the extremely high WSE in 2013, although the simulated discharge matches in--situ observations well (Figure C1~~Figure~~
360 ~~S9~~). This can be well explained by the calibrated curves. The curves at two neighboring cross sections (~~chainage~~XS12 and
XS13~~218.64 and 238.51 km~~) show deviations from the curves derived from surveyed cross sections beyond bankfull depth
(upward curves as shown in Figure 4). Evaluation at two virtual stations also shows good agreements. However, the model

simulation is better than Jason-2 observations except during the 2013 flood bywhen compared referring to the hydrograph of an adjacent gauging stations (Figure 6Figure 6Figure 4).

365
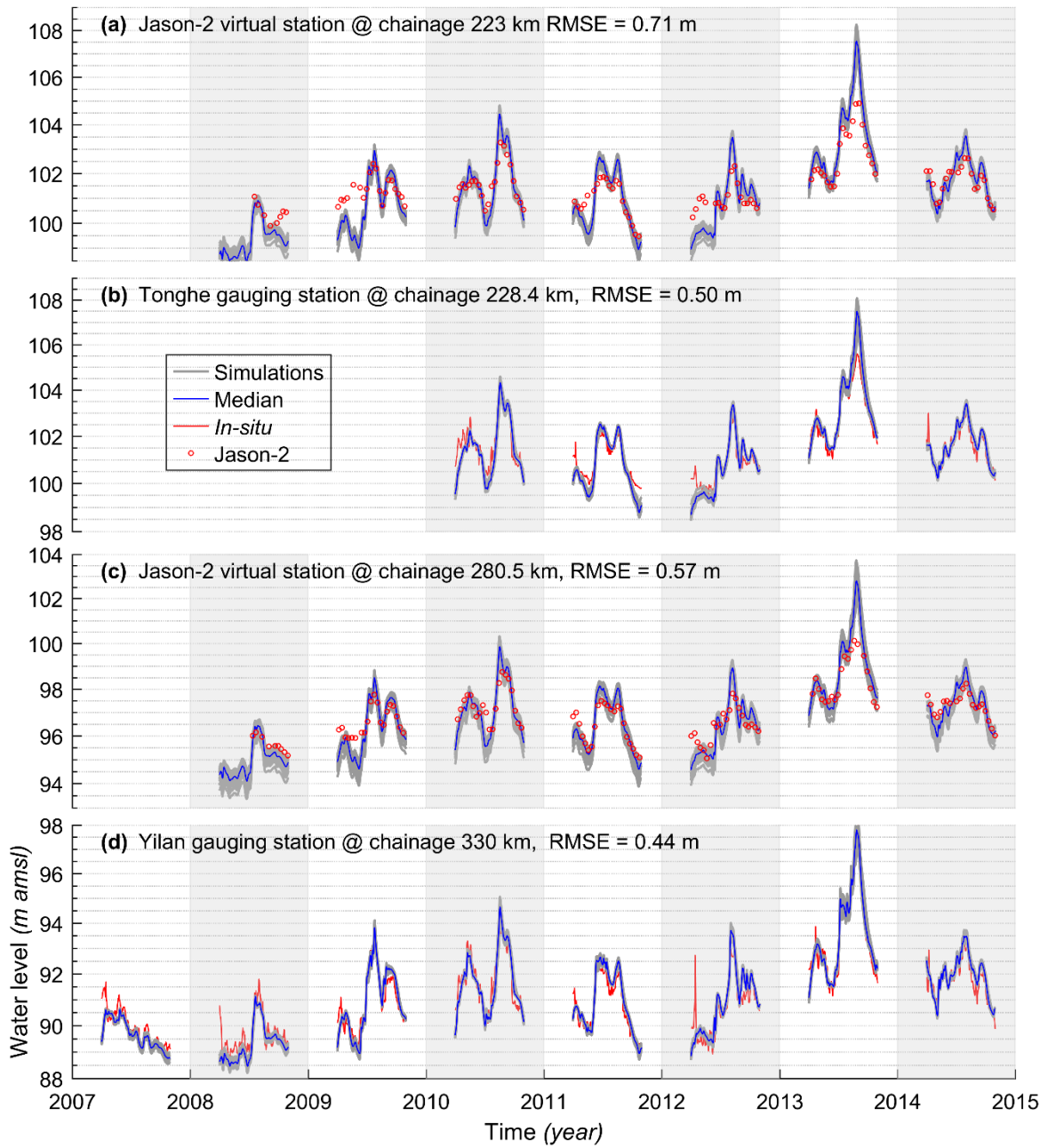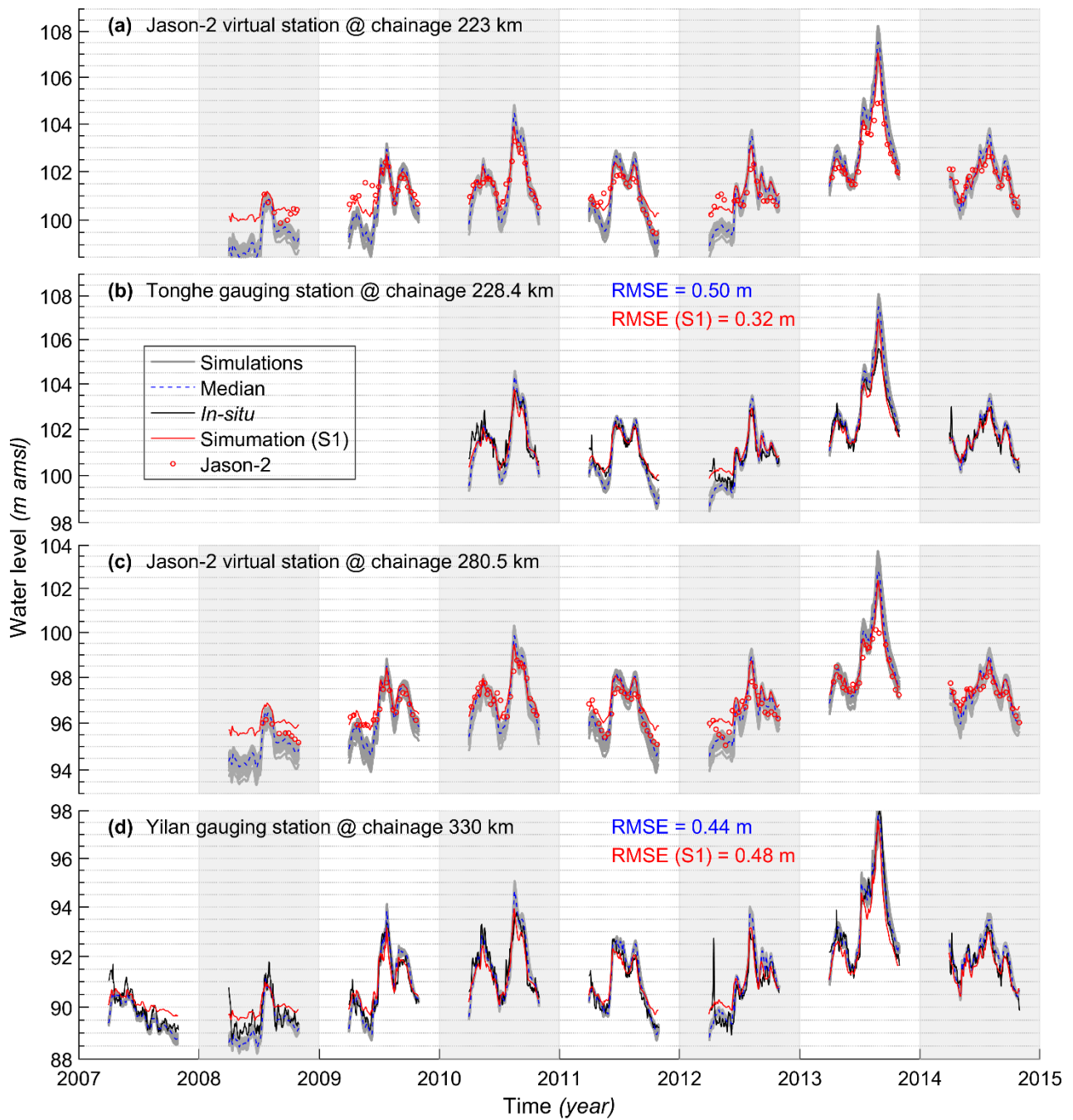
Figure 64. Validation of simulated water level (non-frozen periods) at four stations. (a) and (c) are water levels at two virtual stations, i.e. data derived from Jason-2 altimetry. (b) and (d) are from two stream gauging stations. Simulation from previous model calibrated using different strategy (i.e. simultaneous calibration of roughness and cross-sectional shape parameters) is also shown for comparison. Note, in each plot, results of the median and individual simulations of an ensemble of 30 calibrations (three scenarios of width observations, see Text S3#1, #2, and #3) are shown.

5~~4~~ Discussion

5.1 The value of altimetry and imagery in model calibration

Satellite altimetry data and imagery data have been increasingly used to calibrate hydrologic and hydrodynamic river models (Domeneghetti et al., 2014; Jiang et al., 2019; Liu et al., 2015; Michailovsky et al., 2012; Milzow et al., 2011; Sun et al., 2010). However, joint use of imagery and altimetry for hydrodynamic modeling is not common practice. For our case study, models calibrated with either river width only or WSE only show similar performance in terms of RMSE of WSE at two gauging stations (Figure 5~~Fig. S7~~). However, both cases have problems to fully constrain ~~models~~ parameters and suffer from model ambiguity, which means parameters cannot be well determined. A direct consequence is that model simulations of either the WSE or river width ~~i~~are~~s~~ not physically meaningful (Figure C2~~Fig. S10~~). Because both cases can achieve a reasonable area-depth relationship by making a trade-off between datum and WSE or river width. For example, calibration #1 (WSE only) shows reasonable simulation of WSE (Figure 5), but the simulation of width is not meaningful (Figure 5 and Figure C2). Therefore, both WSE and river width are needed to better constrain model parameters.

Nevertheless, river width and WSE may play different roles in constraining parameters for different rivers depending on the channel shape. If a channel is embanked, for instance, model parameters may not be sensitive to the small changes of river width. This issue certainly needs further investigation. Obviously, observations of river width are easier to obtain and have higher frequency and larger coverage than altimetry-derived WSE (usually the frequency is lower than 10 days). That is, this approach can be applied in many rivers where altimetry data is also available given reliable discharge a~~ts~~ the upstream boundary. This raises a question: Can area and conveyance curves be estimated using short-repeat altimetry missions, such as Jason or Sentinel-3? Our previous study (Jiang et al., 2019) shows that spatial sampling density is more important than temporal frequency in the context of hydraulic inversion and that Jason series alone are not able to constrain the spatially distributed parameters. The trade-off between spatial and temporal sampling density in inland radar altimetry

merits further investigation. Moreover, rapid advances in drone technology also provide WSE and width for small rivers (Bandini et al., 2020). Therefore, this approach is also applicable to rivers where satellite altimetry data are not available. Moreover, further comprehensive investigation of the impact of width observations (i.e. image spatial resolution and temporal distribution, accuracy, etc.) is needed to draw solid conclusions. Ongoing research will employ simultaneous observations of river width and WSE from SWOT for river hydrodynamic modeling.

5.2 Implications for hydrodynamic modeling in ungauged catchments

Lack of river channel bathymetry data restricts application of hydrodynamic modeling to data-scarce river basins. Most continental- or global-scale hydrologic models are coupled with simple routing schemes for simulating surface water transport in the major rivers of the world (Yamazaki et al., 2011). However, at basin scale, without explicit representation of channel geometry, resolving water level dynamic is impossible. Coupling hydrologic models with hydrodynamic river models would better describe the flow dynamics (water depth, water level, discharge, etc.). The new parameterization proposed in this paper can also be used with hydrologic model simulated discharge instead of observed discharge. In this way, water levels along the river channel could be resolved. We performed a preliminary investigation on the effect of simulated discharge errors on inverted area and conveyance curves. Specifically, for the upstream boundary, modelled discharge from a regional rainfall-runoff model is used instead of in-situ discharge (Fig. Figure C3S11). With this setup, the calibrated 1-D hydrodynamic model can reproduce WSE reasonably well (~0.9 m, see Fig. Figure C3S11). The accuracy is comparable to previous studies, such as Domeneghetti et al. (2014) although surveyed cross sections were used in those studies. This finding demonstrates that this approach has great potential to be applied in ungauged river basins. This is in line with the statement by Liu et al. (Liu et al., 2015) that in-situ discharge data may not be necessary for successful hydrologic model calibration. However, more research is needed to incorporate the proposed parameterization into fully coupled hydrologic-hydrodynamic models for ungauged basins.

5.3 Known issues and limitations

The power-law function relationships of flow area / conveyance and flow depth and the corresponding linearity approximation are confirmed in 6 rivers. One may argue that the relationship may not be globally applicable due to the limited number of rivers to validate the relationships. We cannot rebut this argument without collecting a large sample of surveyed cross sections, which is difficult because of data access problems. However, the rivers we used are of diverse sizes (width ranging from a few meters to kilometers) and flow characteristics, and are from different climate zones (Arctic, Mediterranean, and Asian temperate climates). Therefore, we believe that the relationship holds globally, and we call for extensive validation using other rivers. Regarding the linear relationship between the flow area and conveyance curves for each cross section, it is understandable intuitively given that both flow area and conveyance are linearly related to the same variable, i.e. flow depth. At river reach scale, the strong linear relationships between α and γ, β and δ are empirical.

435   As we mentioned, this study only focuses on the main channel and does not account for overbank flow. In the presence of significant floodplains, the linearity of the curve may fail at bankfull depth as seen in Figure 1 ~~Figure 1~~ and Figure 4~~3~~. Consequently, as seen in Figure 6, the model over-estimates extreme flood peak (year 2013). Similarly, one curve may not be able to describe anastomosing rivers that consist of compound channels. To solve this problem, a second curve is needed to describe the overbank flow as suggested by Garbrecht (1990). On the other hand, instead of calibrating the second curve,

440   real data (such as high resolution DEMs, or ICESat-2, etc.) of the non-inundated portion can be used to parameterize the curves or 1D-2D flood inundation modeling can be applied instead. ~~Moreover, this approach assumes that the established curves are time invariable, which is not applicable to rivers with significant bedform changes.~~

In summary, ~~T~~this approach opens up a range of possibilities to simulate and predict flow dynamics in data scarce regions. In addition to simulating WSE as illustrated in previous sections, discharge retrieval is also possible once the slope

445   is known based on established conveyance curves. The future SWOT mission will deliver WSE and slope simultaneously, which can support discharge retrieval using this approach.

~~5~~6 Conclusions

Directly calibrating roughness and cross-sectional geometry of river models is still challenging. In this paper, we propose a~~n~~ ~~new~~ alternative approach ~~parameterization method~~ to calibrate 1-D hydrodynamic river models using altimetry and imagery

450   observations. The workflow is based on the power-law relationships between flow area / conveyance and flow depth, which is not new and has been described half a century ago (Chow, 1959). In this study, we discovered that the two curves are very well correlated, and the relationship is generally independent of rivers. The novelty of this study is that the flow area and conveyance can be inverted directly using spatially distributed observations of WSE and river width given the boundary conditions. In this way, no explicit considerations of roughness and channel geometry are needed to solve for WSE.

455   Our case study demonstrates that the curves can be estimated using solely remote sensing data, and the calibrated hydrodynamic model can reproduce WSE with fairly high precision (ca. 40 - 50 cm). By referring to the results obtained using different parameterization and calibration approach, the simulated water level using current approach is comparable. Further exploration indicates that this approach can be integrated into a hydrologic-hydrodynamic model for studying ungauged river basins.

460   Overall, this study provides an alternative method for hydrodynamic modeling, especially in regions without in-situ river cross-sectional data. Current satellite imagery (Landsat, Sentinel, Gaofen, etc.) and altimetry (CryoSat-2, AltiKa-DF) can support this approach for relatively large rivers. This ~~new~~ approach of parameterization and calibration may prove especially useful for poorly gauged rivers when high resolution data sets are available from the upcoming SWOT mission.

Appendix A: **Supplementary information on the relationships between flow area / conveyance and depth**

465 Take the linear relationships of (A, d) and (K, d), i.e. Eq. (8) and Eq. (9) as the start. Substituting $\log d$ in Eq. (9), we can get

$$\log A = \alpha + \frac{\beta}{\delta}(\log K - \gamma) \tag{A1}$$

By rearranging Eq. (A1), we have

$$\alpha = \log A - \frac{\beta}{\delta}\log K + \frac{\beta}{\delta}\gamma \tag{A2}$$

Further, we can write it as $\alpha = m + n\gamma$ with $m = \log A - \frac{\beta}{\delta}\log K$ and $n = \frac{\beta}{\delta}$.

470 Therefore, α is linearly related to γ although the intercept (m) and slope (n) are not constant. That is, Eq. (A2) is valid at each individual cross section.

Similarly, we divide Eq. (6) by Eq. (7), we can obtain

$$\frac{A}{K} = \frac{a}{c}d^{\beta - \delta} \tag{A3}$$

Taking log transformation and rearranging the equation, that leaves

475 $$\beta = \frac{\log A - \log K + \gamma - \alpha}{\log d} + \delta \tag{A4}$$

Thus, β can also be expressed as a linear function of δ, but with varying intercept.

One should not confuse Eq. (A2) and Eq. (A4) with Eqs. (11) and (12). The formers are derived at individual cross section, while the latter ones are derived by fitting linear functions to cross-sectional parameters at the reach scale.

480
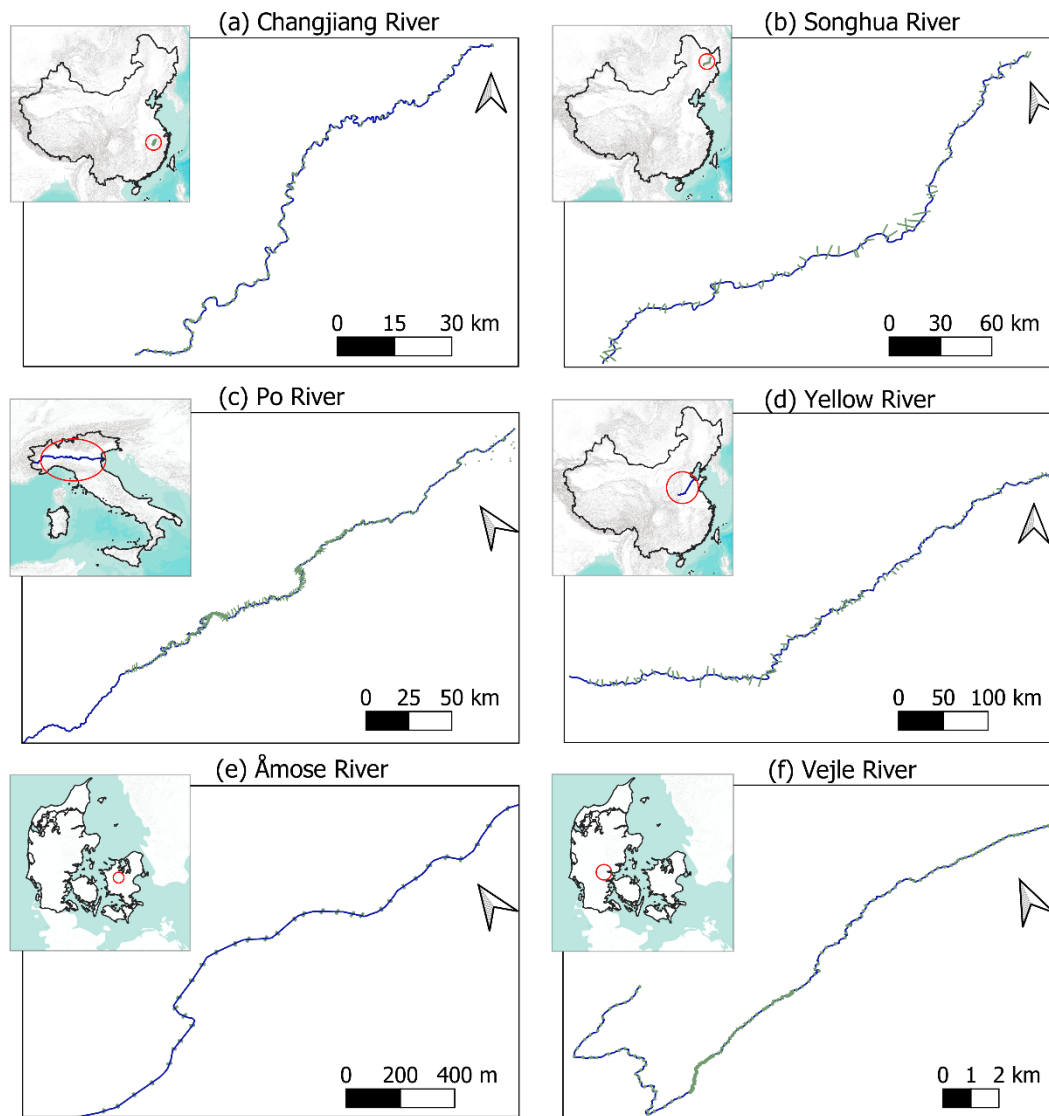
Figure A1. Location and river setting of six rivers. Grey short lines indicate cross sections used to explore the hydraulic relationships.
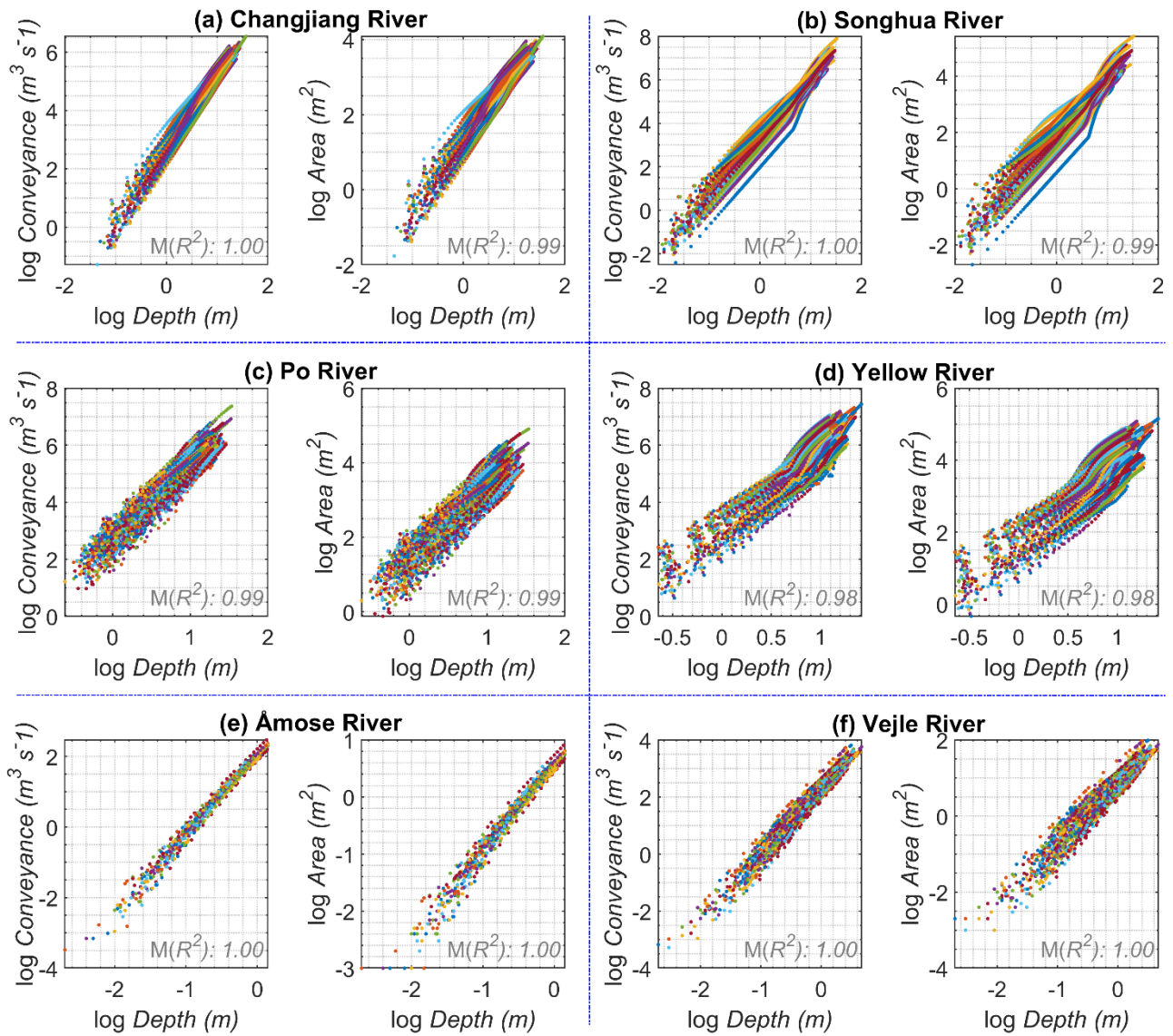
Figure A2. Relationship between logarithmic depth and logarithmic area and logarithmic conveyance. Similar to **Figure 1** but a uniform Manning's number of 0.03 was used to calculate conveyance. This results in a stronger linear relationship. However, a uniform Manning's number is not very realistic in natural rivers.
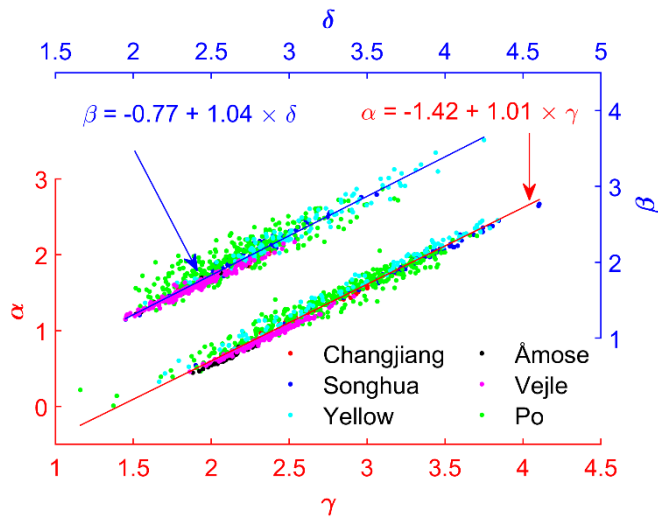
490 **Figure A3.** Linear relationships between gamma ~ alpha and delta ~ beta using data of all six rivers. Similar to **Figure 2**, but a uniform Manning's number of 0.03 was used.
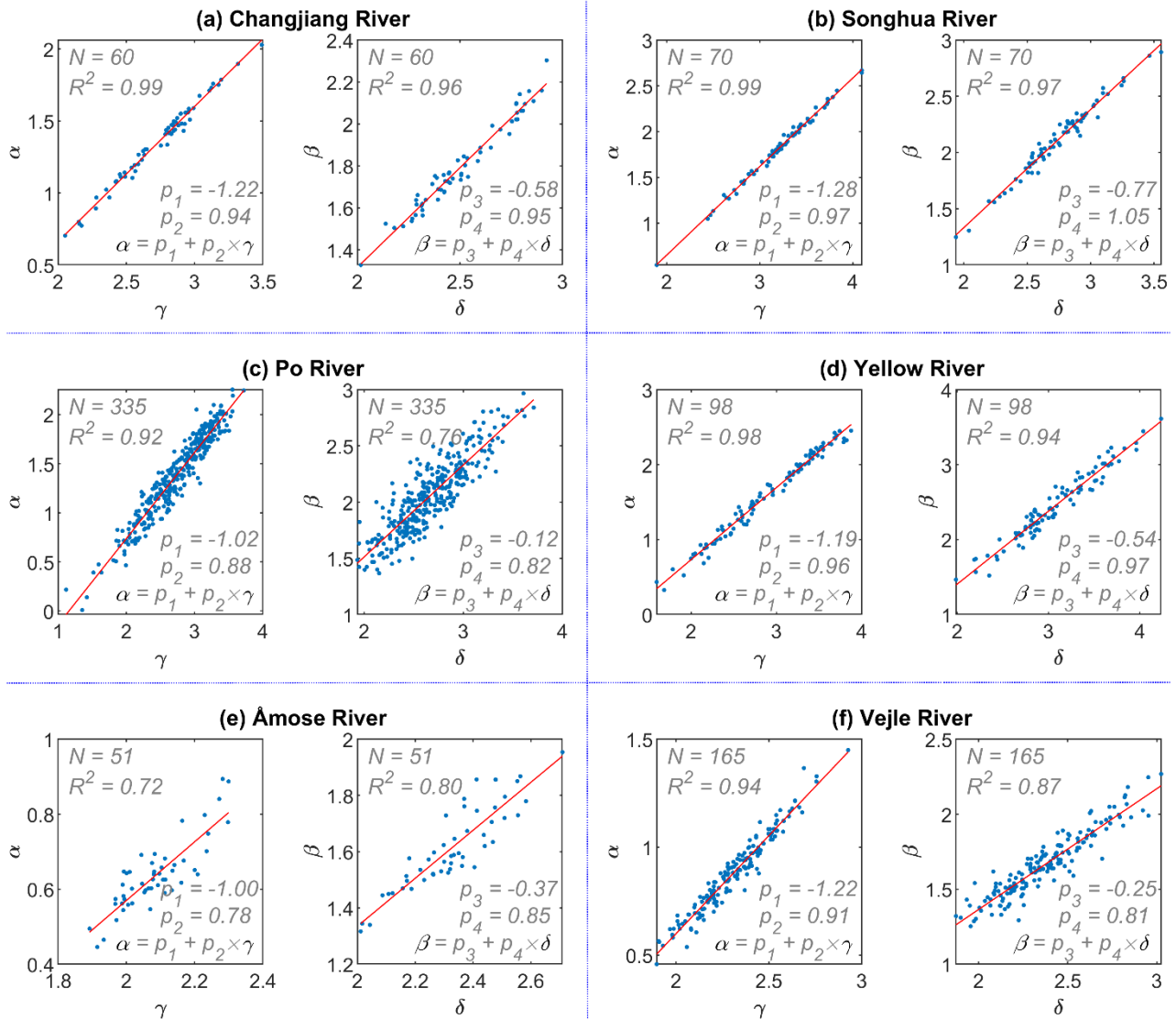
Figure A4. Linear relationships between gamma ~ alpha and delta ~ beta for six rivers. Randomly generated Manning's number in range of 0.015 ~ 0.05 for each cross section was used to calculate conveyance. The number of cross sections, coefficient of determination, and regression coefficients are labelled in each plot.

Appendix B: **Supplementary information on the data sets and calibrated curves**
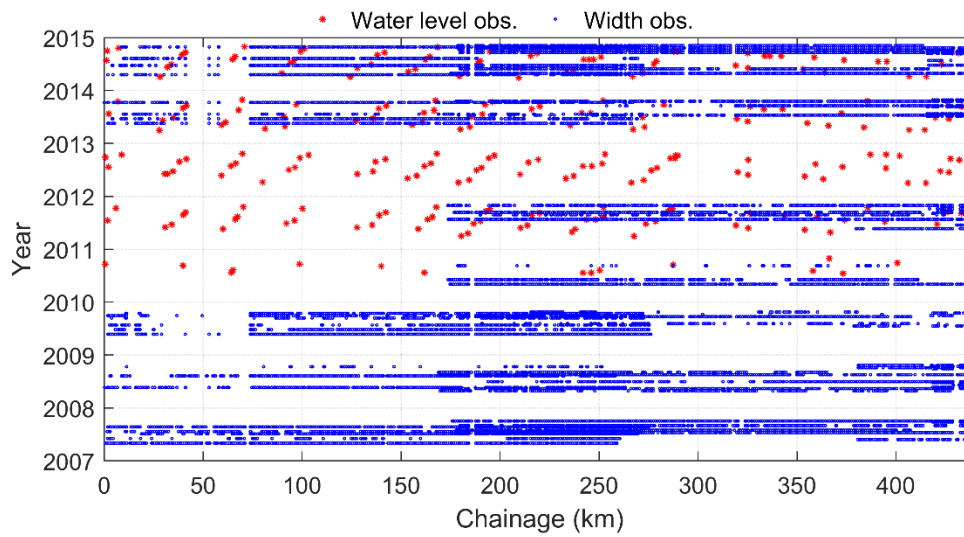
Figure B1. Temporal and spatial distribution of water levels and widths, which are used to calibrate the model. Given that the river is frozen in cold season, only data in warm seasons are used. Landsat-5/8 images with low cloud cover (visual checked in Google Earth Engine) are selected to generate river width.

500
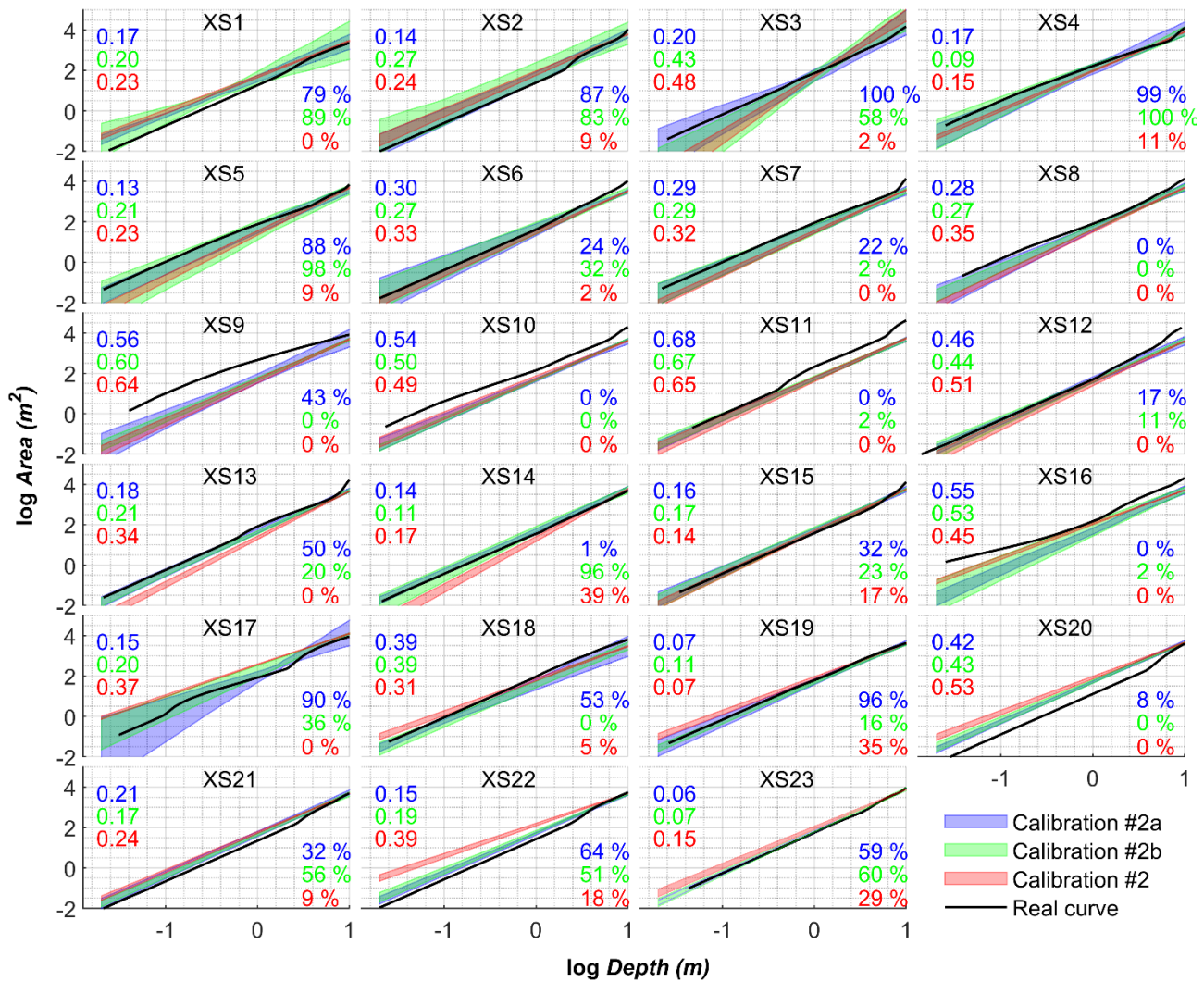
Figure B2. Calibrated curves using three scenarios of width observations only, i.e. one width observation per five-km reach (calibration #2a), one width observation per two-km reach (calibration #2b) and all available widths (calibration #2). The color band represents the mean ± standard deviation based on an ensemble of 10 calibrations. The number of cross section is given in each plot. RMSE and coverage of calibrated curves against real data are reported on the left and right sides of each plot, respectively. Font color is consistent with the curve color. The average RMSE and coverage are 0.28, 0.30, 0.34 and 45%, 36%, 8% for calibration #2a, #2b, #2, respectively.

505
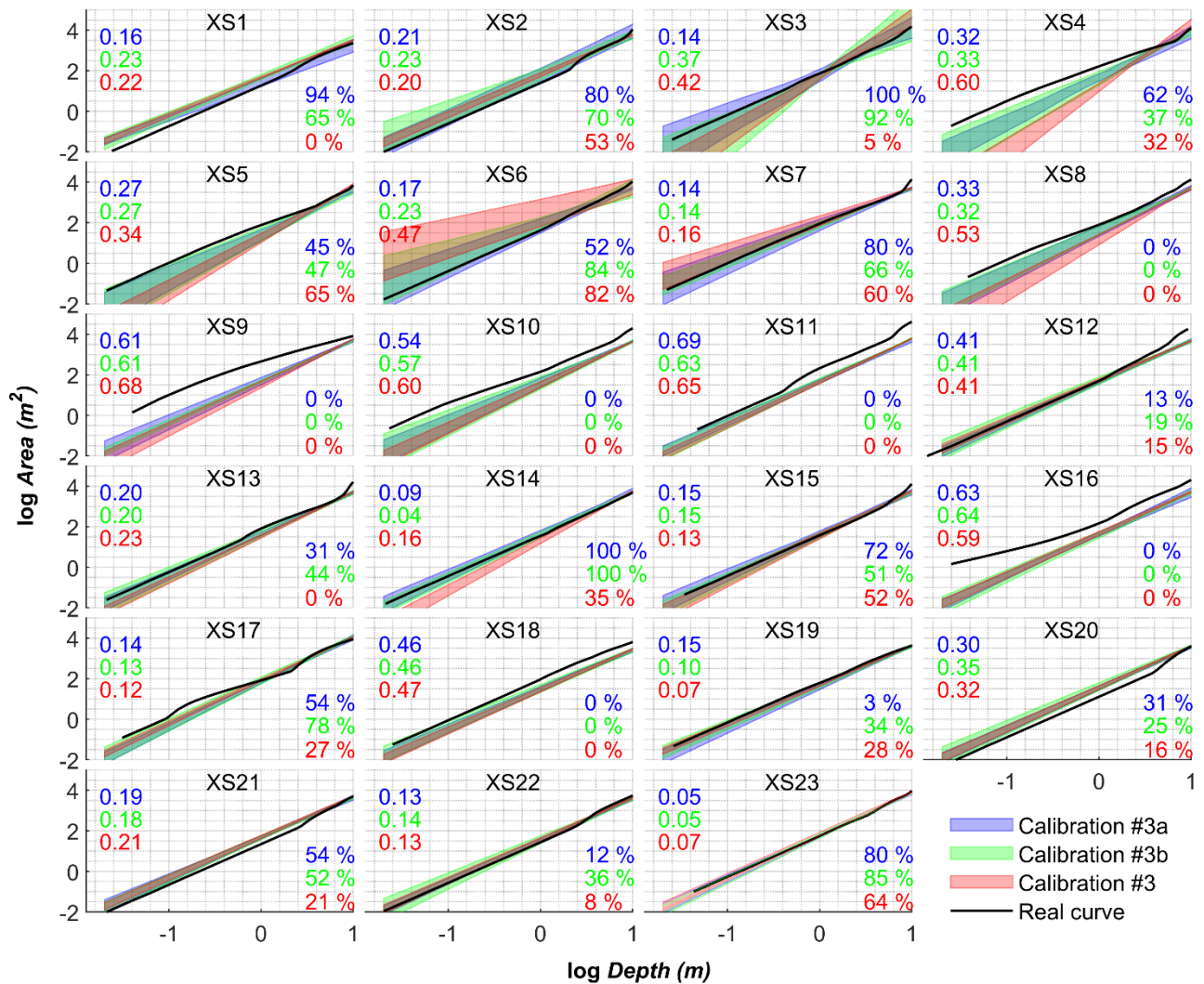
Figure B3. Calibrated curves using **three scenarios of width** observations and water level, i.e. one width observation per five-km reach and water levels (calibration #3a), one width observation per two-km reach and water levels (calibration #3b) and all available widths and water levels (calibration #3). The color band represents the mean ± standard deviation based on an ensemble of 10 calibrations. The number of cross section is given in each plot. RMSE and coverage (percentage of real data falling into the calibrated interval) of calibrated curves against real data are reported on the left and right sides of each plot, respectively. Font color is consistent with the curve color. The average RMSE and coverage are 0.28, 0.29, 0.34 and 41%, 42%, 24% for calibration #3a, #3b, #3, respectively.

Appendix C: **Supplementary information on the simulation results**
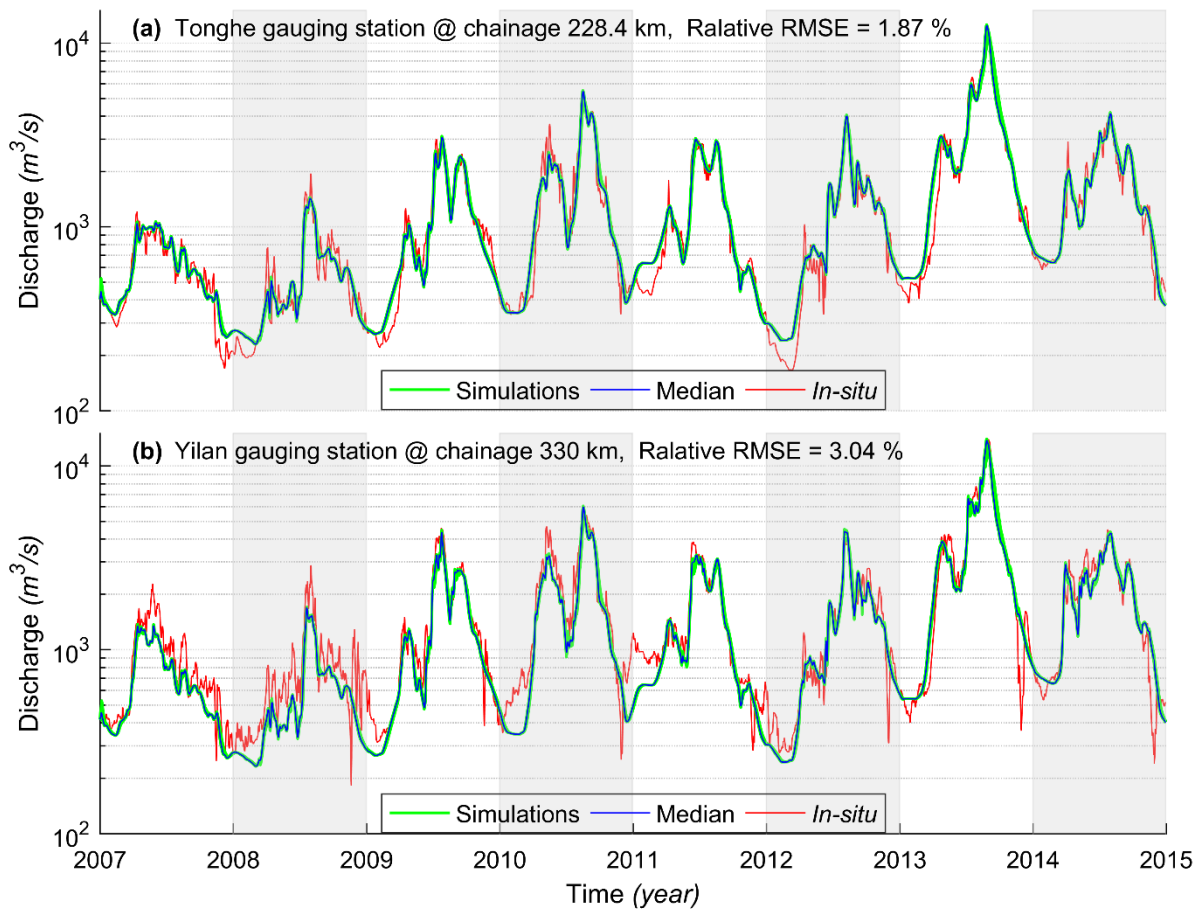
Figure C1. Validation of simulated discharge at two gauging stations. Note, in each plot, results of the median and individual simulations of an ensemble of 30 calibrations (i.e. calibration #1, #2, and #3) are shown.
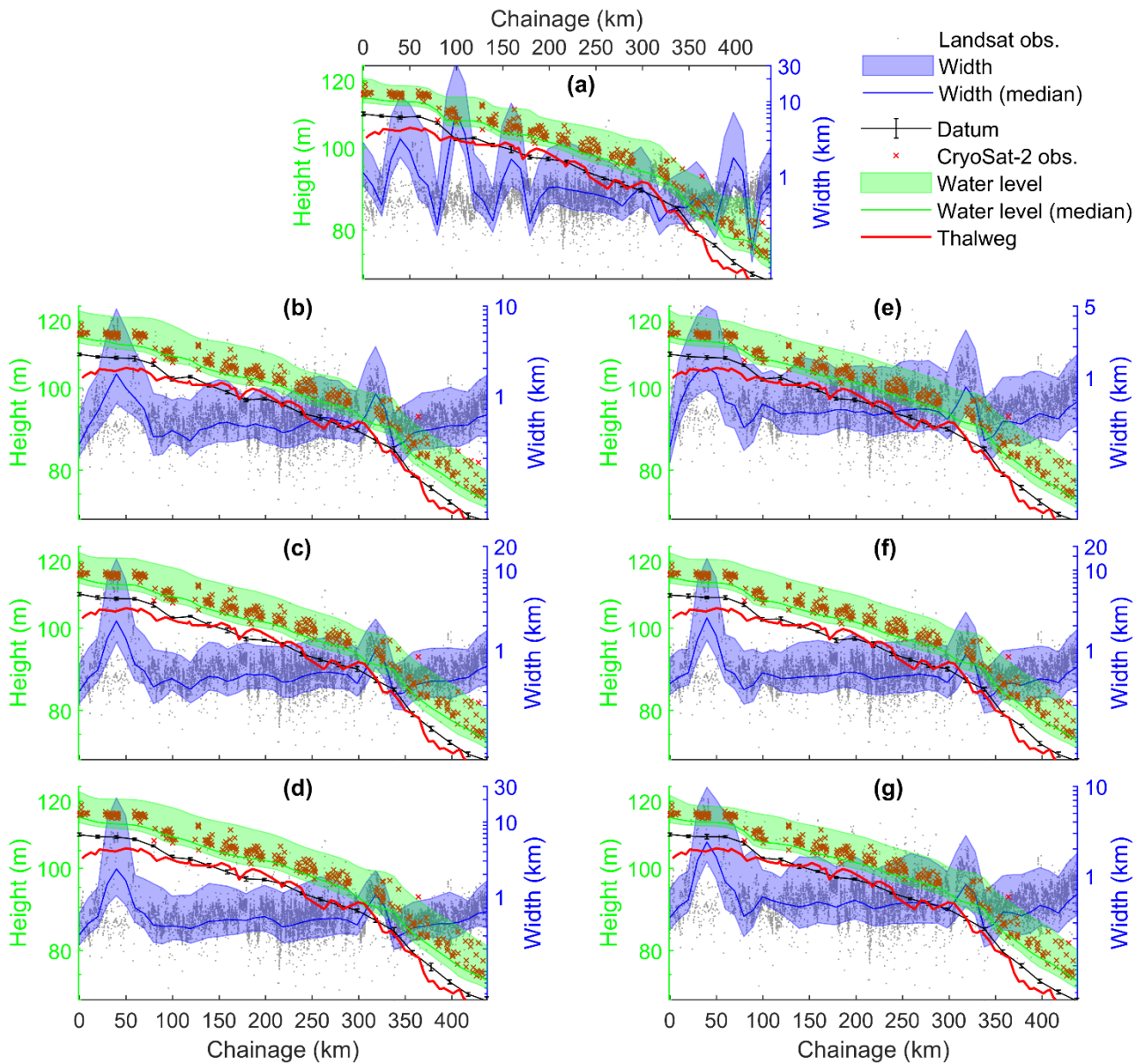
Figure C2. Comparison of model simulated water level, width, and datum using different calibration data sets. (a) calibration #1; (b) calibration #2a; (c) calibration #2b; (d) calibration #2; (e) calibration #3a; (f) calibration #3b and (g) calibration #3. Note, y axes are in log scale. Color bands indicate the boundary (i.e. maximum and minimum) of simulations. Along with model simulations, satellite observations of WSE and width are plotted.
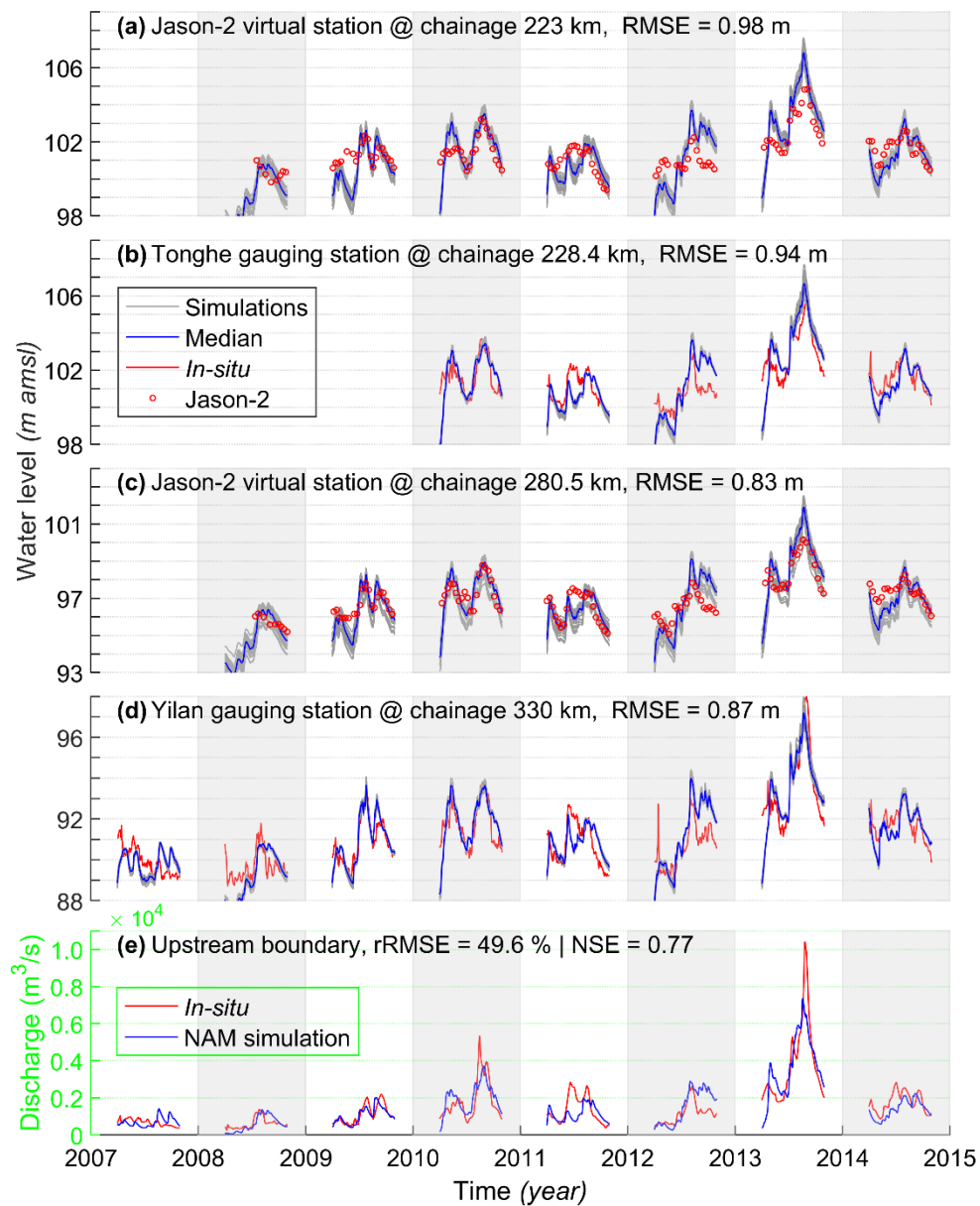
Figure C3. Similar to **Figure 6**, but upstream boundary is rainfall-runoff model simulation instead of in-situ discharge, which are shown in (e). Note that, NAM model was not calibrated at this location.

530 ***Code and data availability.*** River widths were processed on the Google Earth Engine platform. CryoSat-2 were from the study of Jiang et al. (2019). Jason-2 data were downloaded from AVISO+ (https://www.aviso.altimetry.fr/en/data/data-access/ftp.html). Cross-sectional data of the Changjiang, Songhua, and Yellow rivers were excerpted from the Hydrological Yearbook issued by the Ministry of Water Resources, China. Cross-sectional data of the Po river are publicly available from the Interregional agency for the river Po (http://geoportale.agenziapo.it/web/index.php/it/?option=com_aipografd3). Data of

535 the Danish rivers (Åmose, Velje) were kindly provided by WSP (http://www.hydrometri.dk/hyd/).

Author contributions. SWC developed the methodology in an early stage with inputs from LJ and PBG. LJ further developed the methodology, did the data curation, and performed the calibration work. LG prepared the manuscript. All authors contributed to editing the manuscript.

Competing interests. The authors declare that they have no conflict of interest.

540 ***Acknowledgements.*** The authors would like to thank AVISO+, WSP and AIPo for making the data sets available.

Financial support. This work is jointly funded by the Danida Fellowship Centre (File number: 18-M01-DTU) and the Innovation Fund Denmark (File number: 8087-00002B).

545 **References**

Andreadis, K. M. and Schumann, G. J. P.: Estimating the impact of satellite observations on the predictability of large-scale hydraulic models, Adv. Water Resour., 73, 44–54, doi:10.1016/j.advwatres.2014.06.006, 2014.

Annis, A., Nardi, F., Volpi, E. and Fiori, A.: Quantifying the relative impact of hydrological and hydraulic modelling parameterizations on uncertainty of inundation maps, Hydrol. Sci. J., 65(4), 507–523, doi:10.1080/02626667.2019.1709640,

550 2020.

Aster, R. C., Borchers, B. and Thurber, C. H.: Parameter estimation and inverse problems, Elsevier., 2018.

Bandini, F., Sunding, T. P., Linde, J., Smith, O., Jensen, I. K., Köppl, C. J., Butts, M. and Bauer-Gottwein, P.: Unmanned Aerial System (UAS) observations of water surface elevation in a small stream: Comparison of radar altimetry, LIDAR and photogrammetry techniques, Remote Sens. Environ., 237(October 2019), 111487, doi:10.1016/j.rse.2019.111487, 2020.

555 Bates, P. D., Neal, J. C., Alsdorf, D. and Schumann, G. J.-P.: Observing Global Surface Water Flood Dynamics, Surv.

Geophys., 35(3), 839–852, doi:10.1007/s10712-013-9269-4, 2014.

Biancamaria, S., Lettenmaier, D. P. and Pavelsky, T. M.: The SWOT Mission and Its Capabilities for Land Hydrology, Surv. Geophys., 37(2), 307–337, doi:10.1007/s10712-015-9346-y, 2016.

Bierkens, M. F. P.: Global hydrology 2015: State, trends, and directions, Water Resour. Res., 51(7), 4923–4947,
560   doi:10.1002/2015WR017173, 2015.

Bjerklie, D. M., Moller, D., Smith, L. C. and Dingman, S. L.: Estimating discharge in rivers using remotely sensed hydraulic information, J. Hydrol., 309(1–4), 191–209, doi:10.1016/j.jhydrol.2004.11.022, 2005.

Blöschl, G., Gaál, L., Hall, J., Kiss, A., Komma, J., Nester, T., Parajka, J., Perdigão, R. A. P., Plavcová, L., Rogger, M., Salinas, J. L. and Viglione, A.: Increasing river floods: fiction or reality?, Wiley Interdiscip. Rev. Water, 2(4), 329–344,
565   doi:10.1002/wat2.1079, 2015.

Brisset, P., Monnier, J., Garambois, P.-A. and Roux, H.: On the assimilation of altimetric data in 1D Saint–Venant river flow models, Adv. Water Resour., 119, 41–59, doi:10.1016/j.advwatres.2018.06.004, 2018.

Broyden, C. G.: A class of methods for solving nonlinear simultaneous equations, Math. Comput., 19(92), 577–577, doi:10.1090/S0025-5718-1965-0198670-6, 1965.

570   Chow, V. Te: Open channel hydraulics, McGraw-Hill Book Company, Inc, New York., 1959.

Dey, S., Saksena, S. and Merwade, V.: Assessing the effect of different bathymetric models on hydraulic simulation of rivers in data sparse regions, J. Hydrol., 575(March), 838–851, doi:10.1016/j.jhydrol.2019.05.085, 2019.

DHI: MIKE HYDRO River - User Guide, DHI, Copenhagen., 2017.

Dingman, S. L.: Analytical derivation of at-a-station hydraulic–geometry relations, J. Hydrol., 334(1–2), 17–27,
575   doi:10.1016/j.jhydrol.2006.09.021, 2007.

Domeneghetti, A.: On the use of SRTM and altimetry data for flood modeling in data-sparse regions, Water Resour. Res., 52(4), 2901–2918, doi:10.1002/2015WR017967, 2016.

Domeneghetti, A., Tarpanelli, A., Brocca, L., Barbetta, S., Moramarco, T., Castellarin, A. and Brath, A.: The use of remote sensing-derived water surface data for hydraulic model calibration, Remote Sens. Environ., 149, 130–141,
580   doi:10.1016/j.rse.2014.04.007, 2014.

Durand, M., Andreadis, K. M., Alsdorf, D. E., Lettenmaier, D. P., Moller, D. and Wilson, M.: Estimation of bathymetric depth and slope from data assimilation of swath altimetry into a hydrodynamic model, Geophys. Res. Lett., 35(20), L20401, doi:10.1029/2008GL034150, 2008.

Ferguson, R. I.: Hydraulics and hydraulic geometry, Prog. Phys. Geogr. Earth Environ., 10(1), 1–31,
585   doi:10.1177/030913338601000101, 1986.

Fleischmann, A., Paiva, R. and Collischonn, W.: Can regional to continental river hydrodynamic models be locally relevant? A cross-scale comparison, J. Hydrol. X, 3, 100027, doi:10.1016/j.hydroa.2019.100027, 2019.

Fonstad, M. A. and Marcus, W. A.: Remote sensing of stream depths with hydraulically assisted bathymetry (HAB) models, Geomorphology, 72(1–4), 320–339, doi:10.1016/j.geomorph.2005.06.005, 2005.

590   Garambois, P.-A., Calmant, S., Roux, H., Paris, A., Monnier, J., Finaud-Guyot, P., Samine Montazem, A. and Santos da Silva, J.: Hydraulic visibility: Using satellite altimetry to parameterize a hydraulic model of an ungauged reach of a braided river, Hydrol. Process., 31(4), 756–767, doi:10.1002/hyp.11033, 2017.

Garambois, P. A. and Monnier, J.: Inference of effective river properties from remotely sensed observations of water surface, Adv. Water Resour., 79, 103–120, doi:10.1016/j.advwatres.2015.02.007, 2015.

595   Garbrecht, J.: Analytical representation of cross-section hydraulic properties, J. Hydrol., 119(1–4), 43–56, doi:10.1016/0022-1694(90)90033-T, 1990.

Gleason, C. J.: Hydraulic geometry of natural rivers: A review and future directions, Prog. Phys. Geogr., 39(3), 337–360, doi:10.1177/0309133314567584, 2015.

Gleason, C. J. and Durand, M. T.: Remote Sensing of River Discharge: A Review and a Framing for the Discipline, Remote
600   Sens., 12(7), 1107, doi:10.3390/rs12071107, 2020.

Grimaldi, S., Li, Y., Walker, J. P. and Pauwels, V. R. N.: Effective Representation of River Geometry in Hydraulic Flood Forecast Models, Water Resour. Res., doi:10.1002/2017WR021765, 2018.

Jiang, L., Nielsen, K., Andersen, O. B. and Bauer-Gottwein, P.: CryoSat-2 radar altimetry for monitoring freshwater resources of China, Remote Sens. Environ., 200, 125–139, doi:10.1016/j.rse.2017.08.015, 2017.

605   Jiang, L., Madsen, H. and Bauer-Gottwein, P.: Simultaneous calibration of multiple hydrodynamic model parameters using satellite altimetry observations of water surface elevation in the Songhua River, Remote Sens. Environ., 225, 229–247, doi:10.1016/j.rse.2019.03.014, 2019.

Jiang, L., Bandini, F., Smith, O., Klint Jensen, I. and Bauer-Gottwein, P.: The Value of Distributed High-Resolution UAV-Borne Observations of Water Surface Elevation for River Management and Hydrodynamic Modeling, Remote Sens., 12(7),
610   1171, doi:10.3390/rs12071171, 2020.

Larnier, K., Monnier, J., Garambois, P. A. and Verley, J.: River discharge and bathymetry estimation from SWOT altimetry measurements, Inverse Probl. Sci. Eng., doi:10.1080/17415977.2020.1803858, 2020.

Legleiter, C. J.: Calibrating remotely sensed river bathymetry in the absence of field measurements: Flow REsistance Equation-Based Imaging of River Depths (FREEBIRD), Water Resour. Res., 51(4), 2865–2884,
615   doi:10.1002/2014WR016624, 2015.

Leopold, L. B. and Maddock, T. J.: The Hydraulic Geometry of Stream Channels and Some Physiographic Implications, Geol. Surv. Prof. Pap. 252, 57, 1953.

Liu, G., Schwartz, F. W., Tseng, K.-H. and Shum, C. K.: Discharge and water-depth estimates for ungauged rivers: Combining hydrologic, hydraulic, and inverse modeling with stage and water-area measurements from satellites, Water
620   Resour. Res., 51(8), 6017–6035, doi:10.1002/2015WR016971, 2015.

Madsen, K., Nielsen, H. B. and Tingleff, O.: Methods for Non-Linear Least Squares Problems (2nd ed.)., 2004.

Marquardt, D. W.: An Algorithm for Least-Squares Estimation of Nonlinear Parameters, J. Soc. Ind. Appl. Math., 11(2), 431–441, doi:10.1137/0111030, 1963.

Mejia, A. I. and Reed, S. M.: Evaluating the effects of parameterized cross section shapes and simplified routing with a coupled distributed hydrologic and hydraulic model, J. Hydrol., 409(1–2), 512–524, doi:10.1016/j.jhydrol.2011.08.050, 2011.

Mersel, M. K., Smith, L. C., Andreadis, K. M. and Durand, M. T.: Estimation of river depth from remotely sensed hydraulic relationships, Water Resour. Res., 49(6), 3165–3179, doi:10.1002/wrcr.20176, 2013.

Michailovsky, C. I., McEnnis, S., Berry, P. A. M., Smith, R. and Bauer-Gottwein, P.: River monitoring from satellite radar altimetry in the Zambezi River basin, Hydrol. Earth Syst. Sci., 16(7), 2181–2192, doi:10.5194/hess-16-2181-2012, 2012.

Milzow, C., Krogh, P. E. and Bauer-Gottwein, P.: Combining satellite radar altimetry, SAR surface soil moisture and GRACE total storage changes for hydrological model calibration in a large poorly gauged catchment, Hydrol. Earth Syst. Sci., 15(6), 1729–1743, doi:10.5194/hess-15-1729-2011, 2011.

Moramarco, T., Barbetta, S., Bjerklie, D. M., Fulton, J. W. and Tarpanelli, A.: River Bathymetry Estimate and Discharge Assessment from Remote Sensing, Water Resour. Res., 55(8), 6692–6711, doi:10.1029/2018WR024220, 2019.

Neal, J., Schumann, G. and Bates, P.: A subgrid channel model for simulating river hydraulics and floodplain inundation over large and data sparse areas, Water Resour. Res., 48(11), 1–16, doi:10.1029/2012WR012514, 2012.

Neal, J. C., Odoni, N. A., Trigg, M. A., Freer, J. E., Garcia-pintado, J., Mason, D. C., Wood, M. and Bates, P. D.: Efficient incorporation of channel cross-section geometry uncertainty into regional and global scale flood inundation models, J. Hydrol., 529, 169–183, doi:10.1016/j.jhydrol.2015.07.026, 2015.

Nielsen, H. B. and Völcker, C.: IMMOPTIBOX: A Matlab Toolbox for Optimization and Data Fitting, 2010.

Pappenberger, F., Beven, K., Frodsham, K., Romanowicz, R. and Matgen, P.: Grasping the unavoidable subjectivity in calibration of flood inundation models: A vulnerability weighted approach, J. Hydrol., 333(2–4), 275–287, doi:10.1016/j.jhydrol.2006.08.017, 2007.

Pereverzyev, S. S., Pinnau, R. and Siedow, N.: Regularized fixed-point iterations for non-linear inverse problems, Inverse Probl., 22(1), 1–22, doi:10.1088/0266-5611/22/1/001, 2006.

Schaperow, J. R., Li, D., Margulis, S. A. and Lettenmaier, D. P.: A Curve-Fitting Method for Estimating Bathymetry From Water Surface Height and Width, Water Resour. Res., 55(5), 4288–4303, doi:10.1029/2019WR024938, 2019.

Schmidt, M.: Least Squares Optimization with L1-Norm Regularization, Proj. Rep., 98(December), 230–238 [online] Available from: http://people.cs.ubc.ca/~schmidtm/Software/lasso.pdf, 2005.

Schneider, R., Godiksen, P. N., Villadsen, H., Madsen, H. and Bauer-Gottwein, P.: Application of CryoSat-2 altimetry data for river analysis and modelling, Hydrol. Earth Syst. Sci., 21(2), 751–764, doi:10.5194/hess-21-751-2017, 2017.

Schneider, R., Ridler, M. E., Godiksen, P. N., Madsen, H. and Bauer-Gottwein, P.: A data assimilation system combining CryoSat-2 data and hydrodynamic river models, J. Hydrol., 557, 197–210, doi:10.1016/j.jhydrol.2017.11.052, 2018.

Schumann, G., Matgen, P., Hoffmann, L., Hostache, R., Pappenberger, F. and Pfister, L.: Deriving distributed roughness values from satellite radar data for flood inundation modelling, J. Hydrol., 344(1–2), 96–111, doi:10.1016/j.jhydrol.2007.06.024, 2007.

Songliao River Conservancy Commission: The Songhua River, Changchun, China., 2004.

Songliao River Conservancy Commission: Water resources bulletin of Songhua & Liao River, Changchun, China. [online]
660   Available from: http://www.slwr.gov.cn/, 2015.

Sun, W. C., Ishidaira, H. and Bastola, S.: Towards improving river discharge estimation in ungauged basins: Calibration of rainfall-runoff models based on satellite observations of river flow width at basin outlet, Hydrol. Earth Syst. Sci., 14(10), 2011–2022, doi:10.5194/hess-14-2011-2010, 2010.

Ward, P. J., Jongman, B., Salamon, P., Simpson, A., Bates, P., De Groeve, T., Muis, S., de Perez, E. C., Rudari, R., Trigg,
665   M. A. and Winsemius, H. C.: Usefulness and limitations of global flood risk models, Nat. Clim. Chang., 5(8), 712–715, doi:10.1038/nclimate2742, 2015.

Yamazaki, D., Kanae, S., Kim, H. and Oki, T.: A physically based description of floodplain inundation dynamics in a global river routing model, Water Resour. Res., 47(4), doi:10.1029/2010WR009726, 2011.

Yang, X., Pavelsky, T. M., Allen, G. H. and Donchyts, G.: RivWidthCloud: An Automated Google Earth Engine Algorithm
670   for River Width Extraction From Remotely Sensed Imagery, IEEE Geosci. Remote Sens. Lett., 17(2), 217–221, doi:10.1109/LGRS.2019.2920225, 2020.